NASA/CR—2012-217809   Honeywell Report No. 21–13177

Noise Measurements of the VAIIPR Fan

Jeff Mendoza and Don Weir
Honeywell Aerospace, Phoenix, Arizona

December 2012

NASA STI Program . . . in Profile

Since its founding, NASA has been dedicated to the advancement of aeronautics and space science. The NASA Scientific and Technical Information (STI) program plays a key part in helping NASA maintain this important role.

The NASA STI Program operates under the auspices of the Agency Chief Information Officer. It collects, organizes, provides for archiving, and disseminates NASA's STI. The NASA STI program provides access to the NASA Aeronautics and Space Database and its public interface, the NASA Technical Reports Server, thus providing one of the largest collections of aeronautical and space science STI in the world. Results are published in both non-NASA channels and by NASA in the NASA STI Report Series, which includes the following report types:

- TECHNICAL PUBLICATION. Reports of completed research or a major significant phase of research that present the results of NASA programs and include extensive data or theoretical analysis. Includes compilations of significant scientific and technical data and information deemed to be of continuing reference value. NASA counterpart of peer-reviewed formal professional papers but has less stringent limitations on manuscript length and extent of graphic presentations.

- TECHNICAL MEMORANDUM. Scientific and technical findings that are preliminary or of specialized interest, e.g., quick release reports, working papers, and bibliographies that contain minimal annotation. Does not contain extensive analysis.

- CONTRACTOR REPORT. Scientific and technical findings by NASA-sponsored contractors and grantees.

- CONFERENCE PUBLICATION. Collected papers from scientific and technical conferences, symposia, seminars, or other meetings sponsored or cosponsored by NASA.

- SPECIAL PUBLICATION. Scientific, technical, or historical information from NASA programs, projects, and missions, often concerned with subjects having substantial public interest.

- TECHNICAL TRANSLATION. English-language translations of foreign scientific and technical material pertinent to NASA's mission.

Specialized services also include creating custom thesauri, building customized databases, organizing and publishing research results.

For more information about the NASA STI program, see the following:

- Access the NASA STI program home page at *http://www.sti.nasa.gov*

- E-mail your question to *help@sti.nasa.gov*

- Fax your question to the NASA STI Information Desk at 443–757–5803

- Phone the NASA STI Information Desk at 443–757–5802

- Write to:
  STI Information Desk
  NASA Center for AeroSpace Information
  7115 Standard Drive
  Hanover, MD 21076–1320
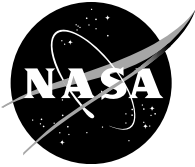
Noise Measurements of the VAIIPR Fan

Jeff Mendoza and Don Weir
Honeywell Aerospace, Phoenix, Arizona

National Aeronautics and
Space Administration

Glenn Research Center
Cleveland, Ohio 44135

December 2012

Acknowledgments

Level of Review: This material has been technically reviewed by NASA technical management OR expert reviewer(s).

Executive Summary and Conclusion

Summary

The VAIIPR program is sponsored by the U.S. Air Force and is administered by Lockheed with the assistance of Honeywell. The VAIIPR program was intend to:

1. Demonstrate the integration of inlet and fan technology
2. Quantify the performance of active flow control (AFC) on performance, operability, and durability
3. Validate inlet and fan computational fluid dynamics (CFD) models.

This test program provided an opportunity to collect information on the impact of inflow distortion on fan noise and to assess the impact of various component interactions with the fan in parallel with planned performance and aeroelastic measurements. The VAIIPR fan has the same aerodynamic design of the rotor and OGVs as the Honeywell TFE731-60.

A circumferential array of sensors was designed to define the modal content of fan noise as generated by the fan interaction with OGVs, struts, upstream struts, IGVs, and various inlet flow distortion conditions due to the serpentine inlet and the introduction of active flow control in the serpentine inlet. The modal decomposition was conducted with a limited number of sensors and therefore required the attempted use of a direction finding technique, previously developed by Honeywell, to resolve a large number of potential interaction modes. This Honeywell direction finding approach is referred to as the Virtual Array.

A sparse array design, defined using Virtual Array processing, with 32 sensors was demonstrated successfully using a simulated pressure field with multiple modes present. The simulated modes were identified out to the rotor alone mode (22 for the 22 bladed fan) but with a compromise in the signal-to-noise ratio. Previous work using a similar array on Honeywell engine data was successful in identifying relevant engine modes. A set of 16 evenly spaced sensors within the sparse array (of 32 sensors) allowed for processing of the data using the more traditional modal processing approach of converting the pressure signal in the space-time domain $p(\theta,t)$ to the wave number-frequency domain $p(m,\omega)$ using a 2-D FFT approach. Due to multiple sensor failures in the sparse array, the 16 sensors making up the evenly spaced array was mostly used to identify the modal content for this program.

Using circumferentially averaged p^2 levels, the measured noise data indicate that AFC in the serpentine inlet provides significant reduction in broadband noise with the reduction occurring gradually with increasing levels of AFC. Active flow control had the effect of eliminating the natural 1/rev distortion from the serpentine inlet and reducing the amount of circumferential distortion at the fan face. Surprisingly, the introduction of AFC slightly increased the levels at the blade pass frequency tone (BPF) and 2xBPF tone. Both findings were consistent for the typical approach, cutback, and max power settings under study. The serpentine inlet provides a significant amount of noise attenuation at high frequencies with less benefit at the BPF. The IGVs were also shown to have the effect of lowering both broadband noise and tone noise as the IGVs closed. This result may be expected because of the drop in fan flow and fan pressure ratio that corresponds to the IGV closing.

Modal results from the evenly spaced sensor array showed a strong presence of a fan IGV interaction. This interaction mode appeared as a dominant aliased mode in the modal decomposition due to the limited spinning mode resolution of the 16 sensor array (–8 to 8). For the test cases where the Virtual Array processing could be utilized, the 32-sensor array clearly identified the presence this $m = –16$ interaction mode from the fan/IGVs. In addition, an $m = 3$ fan/IGV interaction mode was also identified under certain operating conditions. These interaction modes were shown to be reduced significantly in amplitude as the IGVs were closed. At the highest speed setting both arrays showed the presence of an $m = 22$ mode (aliased to an $m = 6$ mode in the 16 sensor array). This mode is potentially due to the rotor locked where the blade tips may be sonic or near sonic speeds. The modal amplitudes at BPF for the 63 and 85 percent speeds increased with the introduction of AFC consistent with the averaged p^2 results

confirming the trends in the spectral data at the blade pass tones. The 75 percent corrected speed (N_c) condition resulted in a more expected reduction in modal amplitude with AFC. An explanation for these trends is currently unavailable.

The modal processing from both the uniformly spaced array of 16 sensors and the non-uniformly spaced array of 32-sensors where viable appears to have reasonably identified interaction modes consistent with potential noise sources in the duct. The strong presence of fan/IGV interaction modes suggests potentially why this arrangement is not utilized in commercial power plants. Absolute modal amplitudes may be suspect due to the poor performance of some and the loss of several sensors throughout the duration of VAIIPR noise testing. To further assess the modal behavior from the VAIIPR noise measurements it may be insightful to reformulate the problem as a beam-forming problem and apply traditional beam-forming techniques to the measured data. This approach would be more amenable to deconvolution methods that may significantly improve array performance.

Contents

List of Tables

List of Figures

Noise Measurements of the VAIIPR Fan

Jeff Mendoza and Don Weir
Honeywell Aerospace
Phoenix, Arizona 85072

1.0 Introduction

This final report has been prepared by Honeywell Aerospace, Phoenix, Arizona, a unit of Honeywell International, Inc., documenting work performed during the period September 2004 through November 2005 for the National Aeronautics and Space Administration (NASA) Glenn Research Center, Cleveland, Ohio, under the Revolutionary Aero-Space Engine Research (RASER) Program, Contract No. NAS3–01136, Task Order 6, Noise Measurements of the VAIIPR Fan. The NASA Task Manager was Joe Grady, NASA Glenn Research Center, Mail Stop 60–6, Cleveland, Ohio 44135. The NASA Contract Officer was Albert Spence, NASA Glenn Research Center, Mail Stop 60–6, Cleveland, Ohio 44135.

This report focuses on the evaluation of internal fan noise as generated from various inflow disturbances based on measurements made from a circumferential array of sensors located near the fan and sensors upstream of a serpentine inlet.

1.1 Objectives

The Versatile Active Integrated Inlet/Fan for Performance & Durability (VAIIPR) program is sponsored by the U.S. Air Force and is administered by Lockheed with the assistance of Honeywell. The test program provided an opportunity to collect internal noise data for various inflow distortion levels and fan interaction noise.

The PRDA VI fan that is planned for the VAIIPR test has the same aerodynamic design for the rotor and outlet guide vanes (OGV) as the Honeywell TFE731-60 engine. The VAIIPR configuration adds inlet guide vanes (IGVs) and upstream struts to the baseline configuration during Builds 4, 5, and 6.

The Compressor Research Facility (CRF) at Wright-Patterson Air Force Base (AFB) does not have the capability to make external measurements of the fan noise. However, measurements of the in-duct noise are possible at the downstream end of the inlet near the fan face. These measurements allow for calculation of the circumferential spinning modes in the duct and determine if the noise source is due to inlet flow distortion, rotor/OGV interaction, rotor/IGV interaction, or rotor/strut interaction. These data could then be compared to the commercial fan configuration for further validation. The data would also be valuable for design tool validation when combined with the currently planned measurements of flow distortion and rotor blade response.

The acoustic test objectives are to determine the effect on fan noise due to:

a. Changes in inlet distortion
b. Introduction of IGVs
c. Introduction of upstream struts
d. Attenuation of the inlet design
e. Smart vane technology

2.0 Background

The primary intent of this program was to quantify the noise impact of various inflow conditions into the fan and potential fan interaction mechanisms resulting from the presence of several upstream and downstream stationary blade rows. This objective was accomplished through teaming with the VAIIPR program on the investigation of fan flow from a serpentine inlet. The VAIIPR program was sponsored by

the Air Force and conducted by Lockheed Martin with the assistance of Honeywell. An objective of the VAIIPR program was to quantify AFC on inlet/fan performance, operability, and durability. Other objectives of the VAIIPR program were to utilize the data to validate integrated inlet/fan CFD models and to assess the effects of angle of attack (AOA) and turning rate with validated analyses. The VAIIPR fan has the same aerodynamic design for the rotor and OGVs as the Honeywell TFE731-60 engine. Honeywell/NASA has an extensive database of TFE731-60 fan noise measurements from the 22-in. rig test at NASA Glenn and the engine validation of noise reduction concepts (EVNRC) testing at Honeywell (see spinning mode content of the TFE731-60 engine in Figure 1). In this figure, the rotor alone mode, m = 22, is clearly identified. The VAIIPR program provided a unique opportunity to assess the noise impact of various inflow distortion conditions into the fan. Noise data was deemed valuable from this fan and serpentine inlet for design tool validation combined with the planned measurements of flow distortion, engine performance, and blade mechanical measurements.

The inflow into a fan from a serpentine inlet typically contains a 1/rev distortion where the low total pressure region is located at the opposite side of the major bend at the inlet to the fan (see example in Figure 2). The serpentine inlet design is largely used in military applications for low radar cross section (RCS) to minimize detectability by inhibiting a direct line-of-sight to the engine hardware. Secondary flow and turbulent boundary layer separation resulting from the bends in the serpentine have been identified as the major contributors to the total pressure distortion from serpentine inlets as discussed in References 1 and 2. The inflow from the serpentine inlet creates a non-uniform pressure field for the compression system to ingest that can result in a decrease in compressor performance, rotating stall, and high-cycle fatigue (HCF) problems, etc. Passive (Ref. 3) and AFC in the serpentine inlet have been utilized to reduce this total pressure loss by countering the inherent secondary flow mechanisms and have proven to be very effective at minimizing the total pressure loss, see Figure 3 for the effect of AFC.
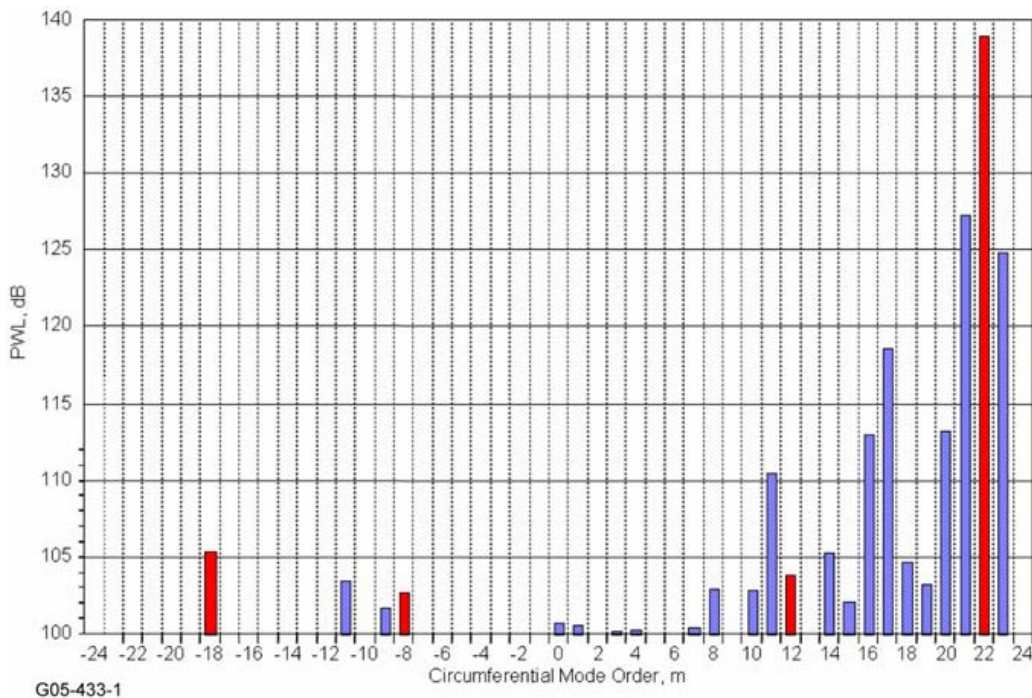
G05-433-1

Figure 1.—Spinning mode content of the Honeywell TFE731-60 engine at a high power setting, rotor alone mode [m = 22] clearly identified.
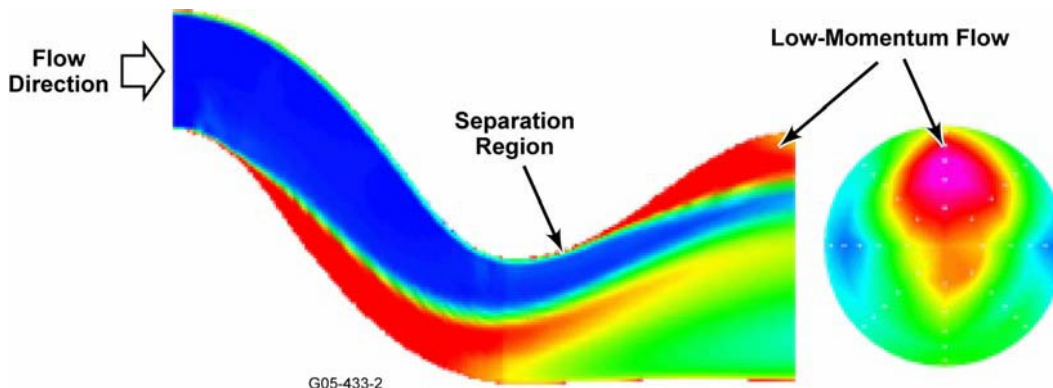
Figure 2.—Inflow distortion from a typical serpentine inlet.
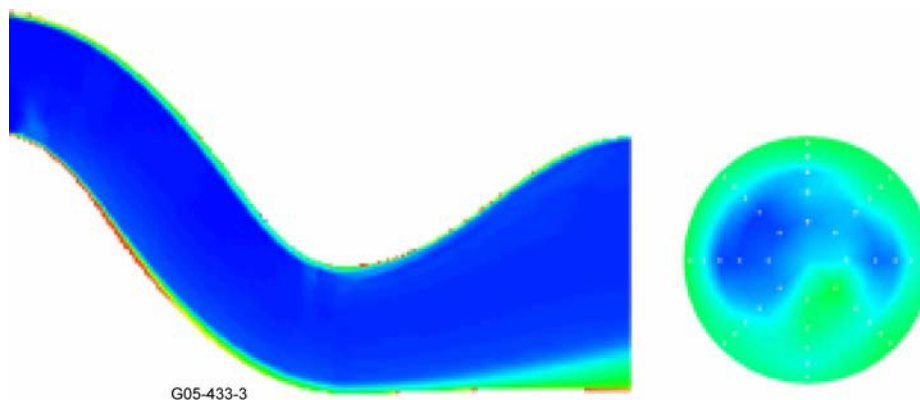
Figure 3.—Inflow distortion from a typical serpentine inlet with flow control.

In addition to the AFC conditions under investigation in the VAIIPR program, the planned engine build configurations for this program provided opportunities to investigate fan interaction mechanisms and the corresponding sound field not generally present in typical turbofan installations. The VAIIPR engine builds and build objectives are summarized in Figure 4. These engine builds were necessary to accomplish the various objectives of the VAIIPR program including CFD calibration, quantifying blade unsteady aerodynamic and vibratory response, and validation of the non-intrusive stress measurement system (NSMS). Acoustic measurements were made during Builds 4A, 5A, and 6. Build 6 (not shown in Figure 4) supports the Smart Vane (IGVs) Program funded by Air Force under a different contract. The smart IGVs were designed by Honeywell and Illinois Institute of Technology to vector the flow into the fan using a novel approach requiring no mechanical articulation. The IGVs were built for use on a Honeywell designed blisk fan rig for performance and operability testing at the Wright Patterson CRF.

Figure 5 shows the blade counts for all stationary and rotating blade components for the Build 4 configuration and identifies the location of the circumferential array of sensors (flow spacer w/ noise sensors) described in sections to follow. As seen in Figure 5, there are a number of potential fan interaction mechanisms. Note that Build 4 is the only configuration where noise data, although limited, was acquired with the three forward struts. The indicated blade counts may be used to help in identifying fan interactions or circumferential spinning mode orders per the Tyler and Sofrin (Ref. 4) description of fan duct mode generation and propagation. There are many possible interaction modes within the VAIIPR fan duct. As reported by the Tyler and Sofrin paper, the generation of circumferential spinning modes is governed by the equation as follows. This equation is used and discussed in later sections of this report to identify fan interaction mechanisms in the measured noise results.

$$m = nB + kV$$

where,
    n = Blade Pass Frequency Index, n = 1, 2, 3,…
    B = Number of Rotor (Fan) Blades
    k = …, –3, –2, –2, 0, 1, 2, 3,…
    V = Vane Blade Count or Interaction Count
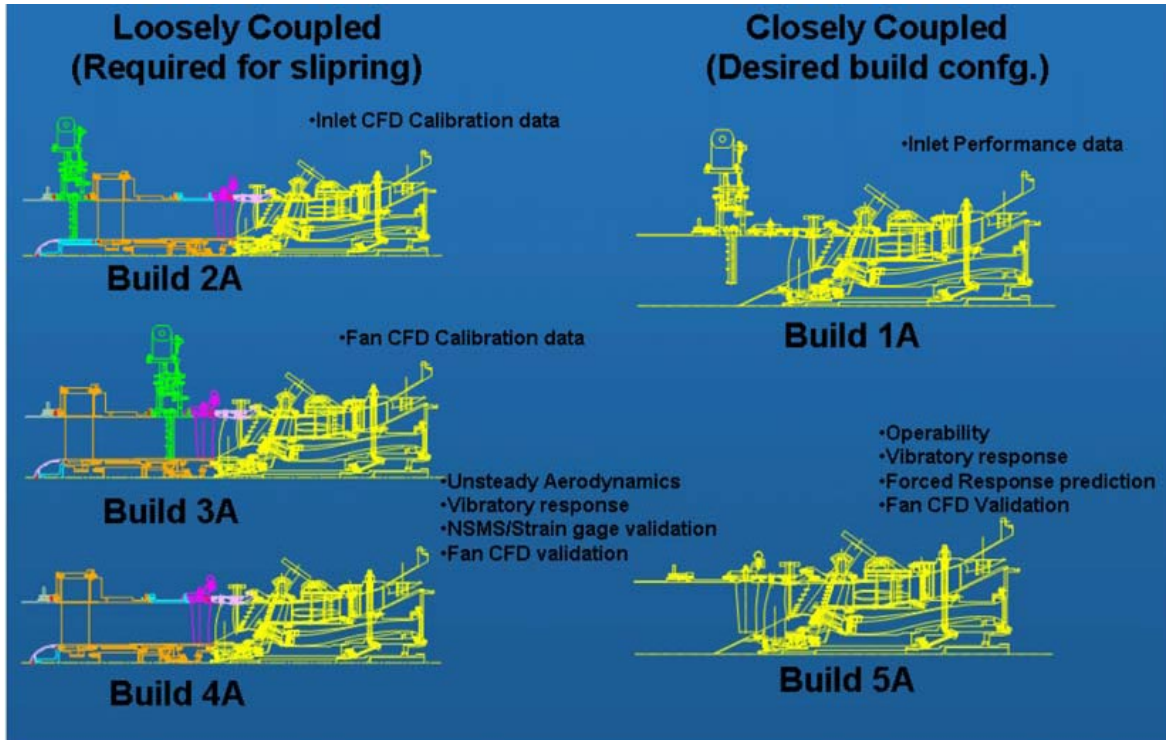
Figure 4.—VAIIPR build summary.
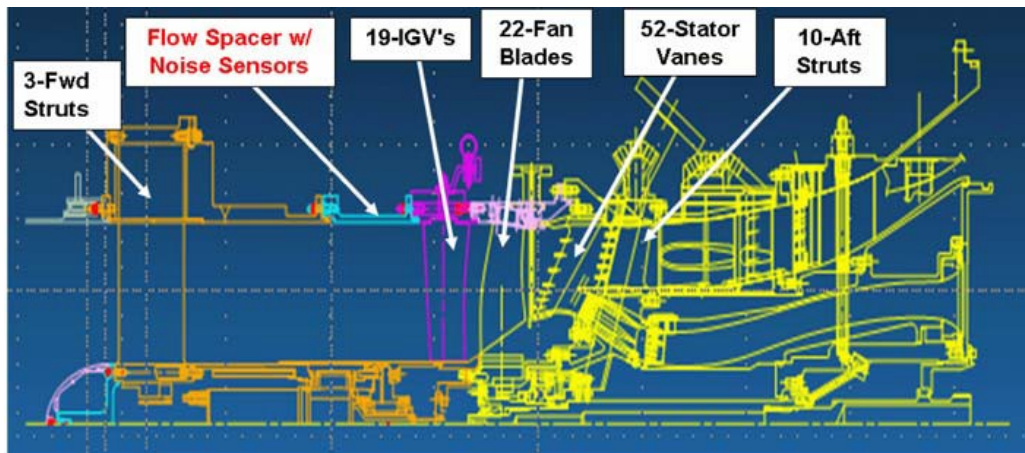
Figure 5.—Engine cutaway identifying engine blade counts and potential interaction mechanisms.

3.0   Technical Approach

3.1   Overall Approach

Aerodynamic tone noise generated by fans occurs at specific frequencies relating to the blade number (count) and rotational speed of the machine, namely, the blade passing frequency and its harmonics and results from the interaction of the unsteady fan blade wakes with other downstream components such as struts or vanes or the interaction of the potential field from these downstream components with the fan rotor. Similarly, the wakes from blades of stationary upstream components or flow distortion can interact with the rotating fan blades to generate similar aerodynamic interaction noise. The mechanisms of fan noise generation are described in much greater detail in References 4 to 6. It is well documented that determining the spinning mode structure or m-order in the engine duct can identify these specific interaction mechanisms or noise sources; see References 7 to 10 for pioneering demonstrations of this measurement concept.

The VAIIPR Fan Noise Measurement Program proposed to quantify the noise sources resulting from inflow distortion, fan/aft strut interactions, fan/stator interaction, fan/IGV interactions, and fan/upstream strut interactions of a serpentine inlet and Honeywell TFE731-60 like fan. The fan design and key parameters are shown in Figure 6. Since the VAIIPR engine test configurations in the CRF at Wright Patterson could not support external far field noise measurements, internal sensors were used to quantify the aforementioned noise sources. This program set out to measure the mode structure near the fan as well as document the sound pressure levels (SPLs) near the fan using an array of internal sensors and sensors at the inlet of the serpentine inlet, see sensor location in Figure 7. Figure 8 shows the VAIIPR engine and inlet configuration in the CRF at Wright Patterson. Indicated in this figure are the locations of the acoustic ring of circumferential sensors, sensor cabling, and data acquisition system. The bellmouth at the entrance of the serpentine inlet was supplied with air by a much larger plenum in the facility.

The approach to achieving these noise measurement goals was to design a circumferential array of sensors able to resolve 22 unaliased modes (the rotor alone mode for the TFE731-60 like fan) to allow for the spatial separation of spinning modes in the duct. A maximum of approximately 32 sensors were available to the VAIIPR Fan Noise Measurement Program. An array design consisting of far fewer sensors (due to sensor availability) than what is traditionally required to adequately cover the desired spinning mode range of m = ±22 was settled on due to this sensor count limitation. A Virtual Array concept utilizing direction finding techniques developed by Honeywell allowed for the attempted use of 32 circumferential array sensors to resolve the mode distribution over the spinning mode range of interest. The Virtual Array of 32 sensors is a sparse array from an array of 48 evenly spaced sensors with 16 sensors removed. The final sensor layout also allowed for the use of a sub array of 16 evenly spaced sensors around the circumference where the more traditional approach using a 2-D FFT could be employed to compute the circumferential spinning modes out to m = ±8. The evenly spaced array of 16 sensors was expected to contain aliasing of the potential interaction modes of interest, e.g., the rotor alone 22 mode should alias to the m = 6 mode in the evenly spaced array. Figure 9 shows the sparse array (circles) and sub array (Xs). These array designs are described in more detail in following sections.

Sensor type, count, and availability were determined in parallel with the design of the circumferential array, i.e., the array design took into account the limited number of sensors available to the program. PCB Piezotronics, Inc. sensors were selected because of the robustness of these sensors, Honeywell's experience with these particular sensors, and availability. Ten 112A22 PCBs and signal conditioning units were provided by NASA LaRC. The remaining 24 112A22 PCBs were provided by Honeywell. The combination of the 32 circumferential array sensors, two sensors in the inlet of the serpentine inlet, and the 1/rev signal required a minimum of 35 channels of simultaneous data acquisition.
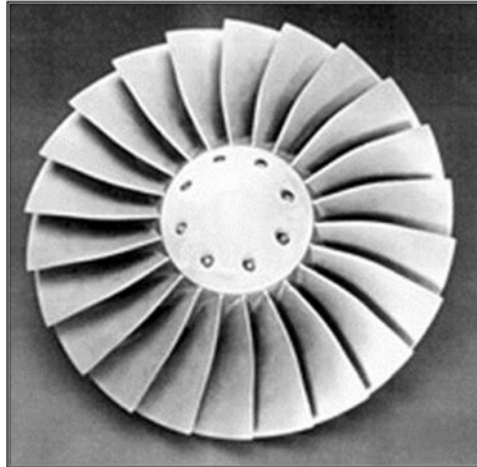
Tip Rel Mach Number	1.502
LE Tip Diam (in)	17.756
LE Hub-Tip Ratio	0.35
Tip Chord (in)	3.733
Tip Stagger (deg)	60.93
Aspect Ratio	1.33
Mean Solidity	1.862
Corr Tip Speed (ft/s)	1474
Inlet Spec Flow (lbm/s*ft^2)	42.27
Max Steady Stress at MDP (ksi)	91.4
Max Physical Speed (rpm)	17589
Design Corrected Speed (rpm)	19032
Design Corrected Flow (lbm/s)	64.32
Design Rotor Pr (overall)	1.824
Design Rotor Eff (overall)	91.43
Number Rotor Blade	22
Number Stator Vanes	52
Number Struts	10

G05-433-6

Figure 6.—VAIIPR fan design and key design characteristics.
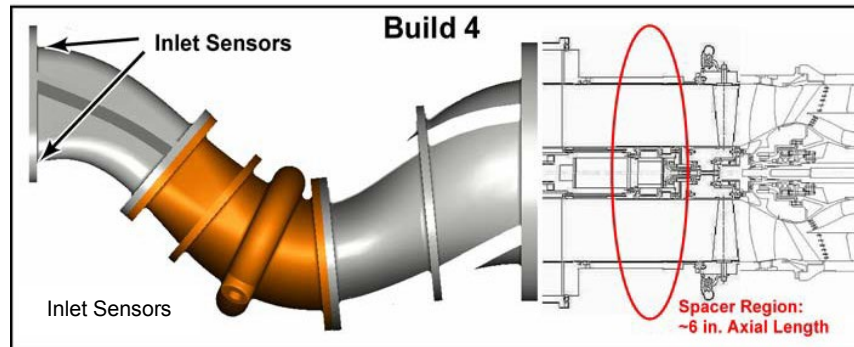
G05-433-7

Figure 7.—Build 4 rig configuration indicating the relative location of the flow spacer and inlet sensors.
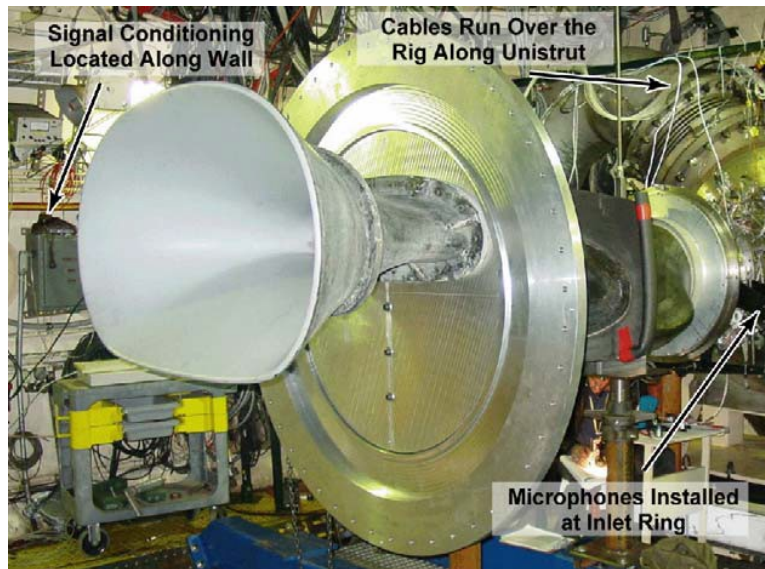
G05-433-8

Figure 8.—Compressor Research Facility (CRF) with VAIIPR engine and serpentine inlet at Wright-Patterson.
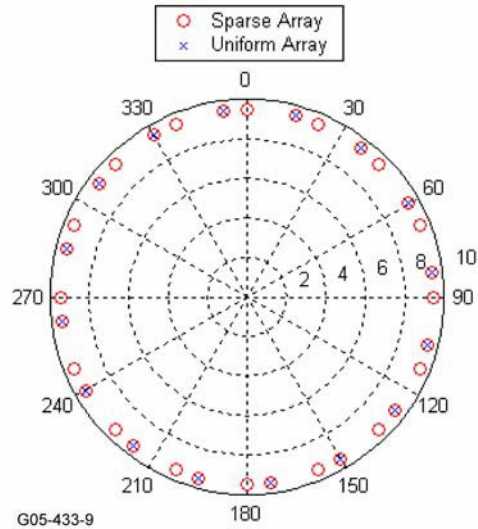
Figure 9.—Array designs for VAIIPR noise measurements.

A data acquisition system was ultimately leased from Dewetron (DEWE-4010) for simultaneous recording of the pressure sensors and 1/rev signal. A 48-channel DEWE-4010 digital recording system was leased due to its compatibility with other Honeywell-owned DEWETRON systems (lower channel counts) and its availability in a relatively short time period. The system availability was critical because of schedule changes in the VAIIPR engine testing. The measurement system was configured with ICP modules and to allow for remote authority of the data acquisition system. The acquisition device was located in the test cell near the sensors and engine hardware, but controlled and viewed from a laptop in the Air Force CRF control room using an Ethernet connection. This remote configuration eliminated the need for 150 ft BNC cables and the potential signal quality issues with such cable lengths. The built-in ICP modules in the DEWE-4010 eliminated the need for external signal conditioning boxes.

Hardware supporting the test instrumentation was designed and fabricated. A ~6-in. flow spacer ring and PCB sensor plugs and solid plugs (sensor removed) were designed and fabricated to hold the circumferential array of sensors (see Figure 10 and Figure 11). The flow spacer was designed considering the importance of proper alignment of the sensor in the flow path, air sealing, and proper flow path alignment with the rest of the rig. Also, relative sensor positions were critical and all hole centers were located relative to the 12 o'clock sensor position (Sensor 1). The sensor probe holders were fabricated using TEFLON material to thread into the flow spacer and provide electronic shielding. The flow spacer ring was positioned at an axial location approximately 8 in. upstream of the fan face and 4 in. upstream of the IGV leading edge plane. Honeywell worked with the Lockheed Martin and Air Force CRF team to include this flow spacer in the relevant engine builds for noise testing. In addition, Honeywell provided Lockheed Martin with drawings early in the serpentine inlet fabrication process to mount a boss at the 12 o'clock position and one at the 6 o'clock position (forward looking aft) at the inlet to the serpentine inlet (see Figure 12). The sensor bosses secured the flush-mounted pressure sensors at the inlet position.
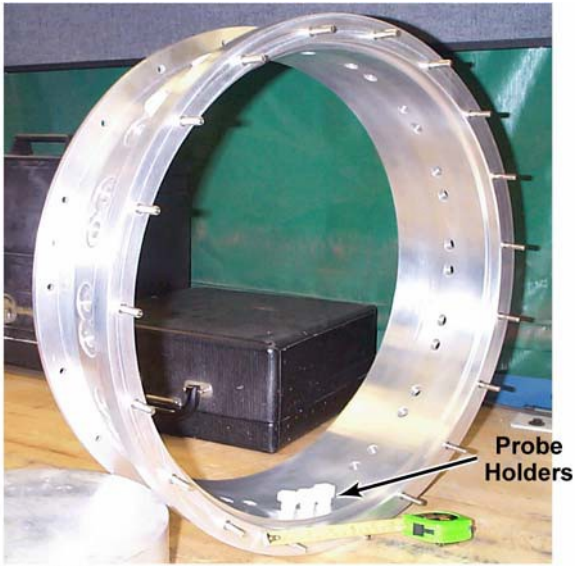
Figure 10.—Outer flow spacer for noise measurement instrumentation.
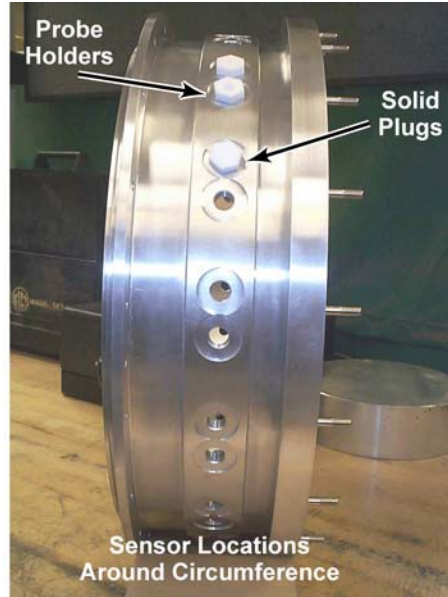
Figure 11.—Side view of outer flow spacer with probe holders and solid plugs.
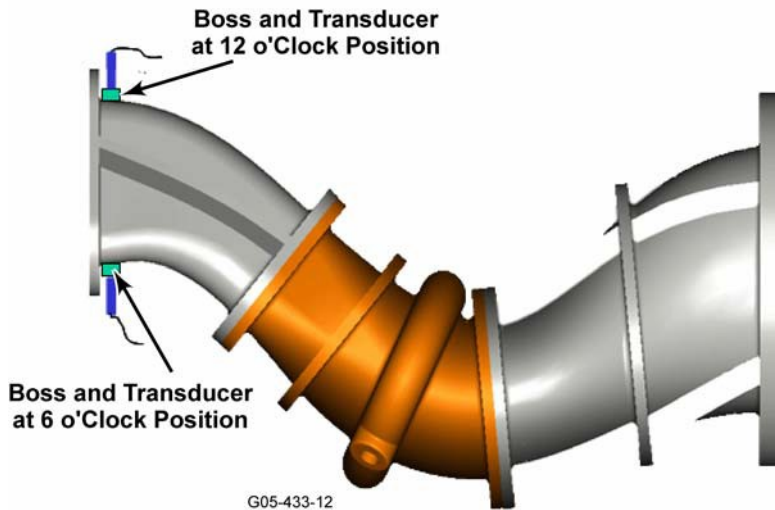
Figure 12.—Inlet sensors at the inlet of the serpentine inlet.
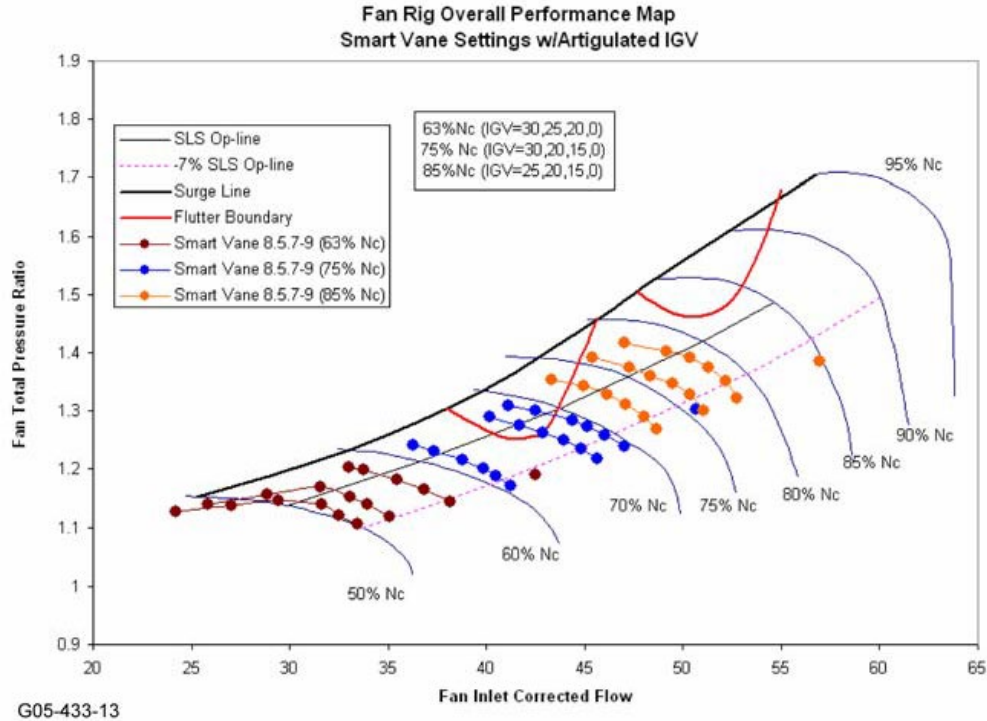
Figure 13.—Summary of engine operating conditions for noise recording.

Honeywell participated in the initial set-up of hardware, instrumentation, and data acquisition equipment. Honeywell acoustics personnel were onsite to support testing during the initial noise measurements, VAIIPR Build 4. Detailed instructions of remote acquisition were provided to Wright Patterson personnel and an acoustic test matrix was provided to identify engine operating conditions for noise recordings during Engine Builds 4, 5, and 6. The engine operating conditions of the VAIIPR program are summarized in Figure 13. Most of the acoustic data were recorded at conditions near the −7 percent op-line (dashed pink line) at speeds of 63, 75 and 85 percent N_c. The baseline IGV settings for these speed settings were 0, 14, and 12 percent, respectively. Noise recordings were made for similar engine operating conditions for the Smart Vane Program. All measured noise data from these engine builds were then downloaded from the Dewtron data acquisition system to an external hard drive and processed at Honeywell in Phoenix.

The follow subsections provide additional details of the array design effort and testing conducted in the CRF at Wright Patterson. There were two key considerations in the array design:

1. There were only ~32 sensors available for the circumferential array.
2. The design must consider the potentially large number of interactions (spinning modes) present due to the many stationary engine components and the inlet distortion harmonics.

3.2   Virtual Array Design

A Virtual Array concept for spinning mode detection was developed to improve Honeywell Engines ability to efficiently make modal measurements of fan noise inside an engine duct. The Virtual Array concept was developed by Honeywell Labs (Corporate R&D) in collaboration with Honeywell Aerospace with the intent of extending the capability of current signal processing methods to estimate larger range of modes than what is typically possible to estimate using traditional methods, 2M sensors required to measure ±m modes. The virtual array technique augments the actual sensor array with virtual sensors placed among the actual sensors to construct a larger virtual array with larger manifold capabilities. This technique can be used for either uniform or non-uniform spaced microphones and was intended to realize

larger unaliased modes with fewer sensors, simplify the measurement task by eliminating the need for traversing sensors, and tolerate a limited number of dead microphones without jeopardizing the system performance.

Subspace methods are straightforward, robust algorithms for high resolution spinning mode estimation and direction finding in general. These methods included Music, Min-Norm, Root-Music and are of interest because they generally outperformed spectral methods, i.e., Beamforming (Ref. 11) and others, in resolving very close emitters. The Root-Music reads off the signal direction from the arguments of the roots of a polynomial. The technique is usually applied to a uniform array of microphones. It is a more direct version than the spectral version, based on the fact that a signal root tends to drift radially inside the unit circle, thus preserving its direction angle even at low signal to noise ratio (Ref. 12). Music on the other hand, is based on a scalar measure of the distance between the array manifold and the estimated noise subspace. Music is known for its robustness to noise drift into the signal subspace. Therefore, it is usually a good candidate for estimation of direction finding in the case where the actual number of modes is not known. The primary concern for all of these methods in estimating the fan spinning modes is the limitation of the range of modes, which is restricted by the size of the array in the acoustic measurement. The Virtual Array concept involves the insertion of virtual sensors into the actual sensor array to construct a larger array and hence, increase the span of the modes that can be estimated without running into the aliasing problem. The virtual array approach involves mapping the problem from the sensor domain into a virtual domain with a larger array manifold. This technique was previously developed under Honeywell funding and designated as a Honeywell Trade Secret, therefore the detailed derivation of the concept has been omitted. Figure 14 shows a sensor layout containing virtual sensors (light blue) and actual sensors (red) in a Honeywell fan rig where the Virtual Array concept was successfully demonstrated.

Using the Virtual Array concept, simulations in MATLAB were conducted to optimize the circumferential array design and sensor placement in the array for the VAIIPR noise program. In an attempt to avoid spatial aliasing with a small number of microphones, the Virtual Array concept was designed to resolve >44 spinning modes in the duct with ~32 available sensors. Sample results are illustrated in Figure 15 where a spinning mode pressure pattern containing the 22, 8, and –15 modes with equal power and an arbitrarily assigned phase distribution was simulated. To right in Figure 15 is the corresponding array sensor locations for the two estimates. Contained in this figure are the spectral estimates of the modal pattern in the duct, assuming the full suite of 48 sensors to resolve –23 to +24 modes compared to a virtual array design using only 32 sensors of the total 48 available. As seen, the virtual MUSIC approach clearly identifies the simulated modes [22, 8, –15] but the signal-to-noise ratio has been degraded. Additional simulations were run to optimize the sensor placement in an attempt to improve the signal-to-noise ratio observed in Figure 15 with no real drastic improvement to the performance. Thus, the array design was set and is shown in Figure 16 along with sensor numbering and polar positioning relative to an observer forward of the fan looking aft.
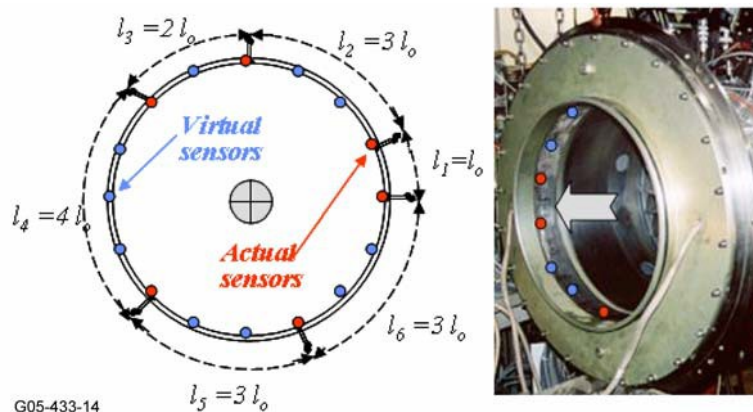
Figure 14.—Honeywell fan rig with actual (red) and virtual array (light blue) of sensors.
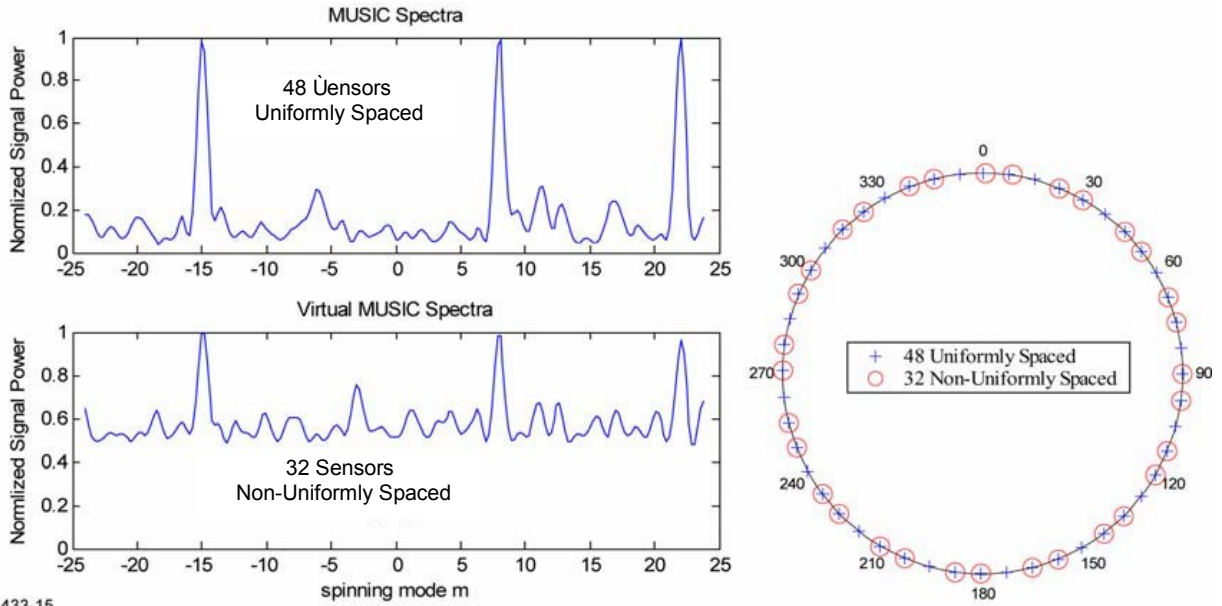
Figure 15.—Virtual array design showing positive identification of simulated modes [22, 8, −15] using only 32 of the available 48 uniformly spaced sensors.
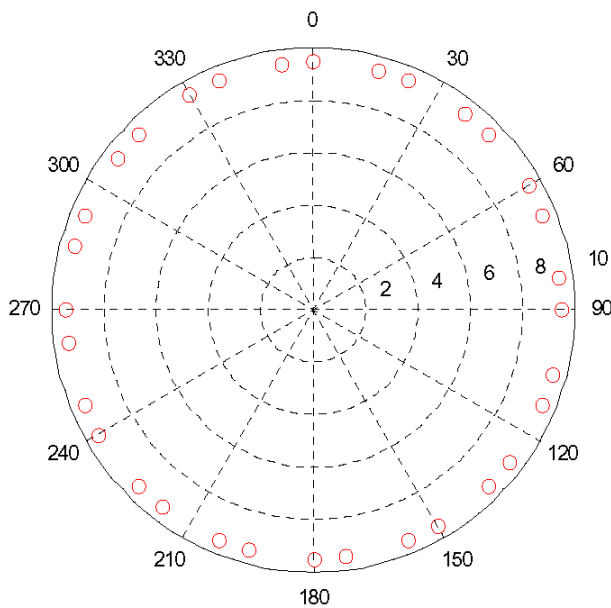
Forward Looking AFT	
Sensor Number	Circumferential Location (Degrees)
1	0.0
2	15.0
3	22.5
4	37.5
5	45.0
6	60.0
7	67.5
8	82.5
9	90.0
10	105.0
11	112.5
12	127.5
13	135.0
14	150.0
15	157.5
16	172.5
17	180.0
18	195.0
19	202.5
20	217.5
21	225.0
22	240.0
23	247.5
24	262.5
25	270.0
26	285.0
27	292.5
28	307.5
29	315.0
30	330.0
31	337.5
32	352.5

Figure 16.—VAIIPR array design with senor numbering and polar placement as indicated.

3.3   Conventional Modal Processing

As previously indicated, two modal processing techniques were used for this program, a sparse array with the Honeywell-developed MUSIC algorithm and a more conventional uniformly spaced array utilizing the traditional 2-D FFT approach to achieve the modal decomposition. Figure 9 shows this subarray of 16 sensors uniformly spaced around the circumference at 22.5° increments (x's) embedded in the 32 sensor sparse array of non-uniformly spaced locations. The initial sensor in the subarray is clocked 7.5° counter clockwise [forward looking aft (FLA)] from the 12 o'clock position. The FFT method of modal decomposition is a process that transforms the pressure field in the space-time domain p(θ,t) to the wavenumber-frequency domain p(m,ω) where θ represents the circumferential angle, t is time, m is the spinning mode order, and ω is the radial frequency. Figure 17 summarizes the Honeywell process beginning with the time histories of the measured pressure field at each sensor position (evenly spaced) in the array. Steps 1, 3, and 5 from the process described in Figure 17 are illustrated in Figure 18 through Figure 20, respectively. Figure 20 shows the modal decomposition results at all engine orders (EOs) or frequencies. The results focus primarily on the response at BPF.

The time domain averaging is intended to emphasis the components of the noise that is coherently related to the shaft rotation. This coherent extraction of the shaft harmonics is achieved by using the measured 1/rev signal to trigger the ensemble averaging such that for a fixed record length each ensemble is initiated at the same starting point in the shaft rotation. Figure 21 shows a typical pressure signal, the first record of the time trace and the ensemble average of the pressure signal, with the 1/rev high amplitude pulses separated by approximately 170 units in the figure. The 1/rev signal was recorded off the spinner using reflective tape or off the gearbox. Both 1/rev signals were found to be sufficient for modal processing when functioning appropriately. The ensemble averaging removes much of the noise and contribution from non-shaft related sources.

1 Time Domain Ensemble Average of Pressure Data at All Sensor Locations

2 Apply Hanning Window to Records

3 Compute Time Domain Discrete Fourier Transform to Records

4 Compute Spatial Domain (Sensor Position) Discrete Fourier Transform

5 Extract Model Amplitudes at the Appropriate Frequency
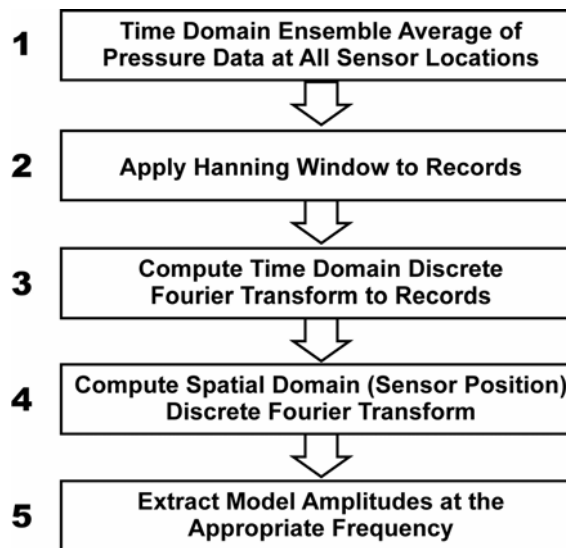
G05-433-17

Figure 17.—Summary of 2-D FFT processing for converting from space-time domain to the wavenumber frequency domain.
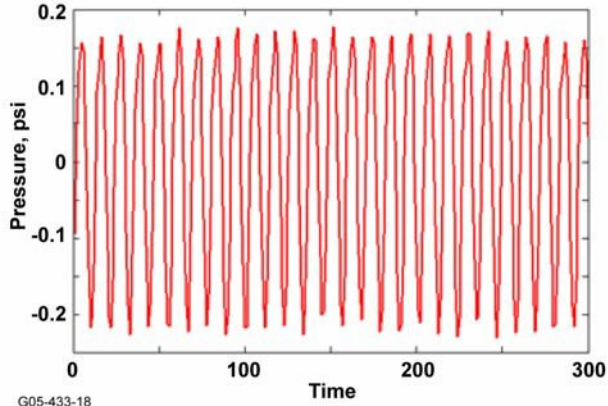
Figure 18.—Typical pressure time history with 1000+ ensemble averages.
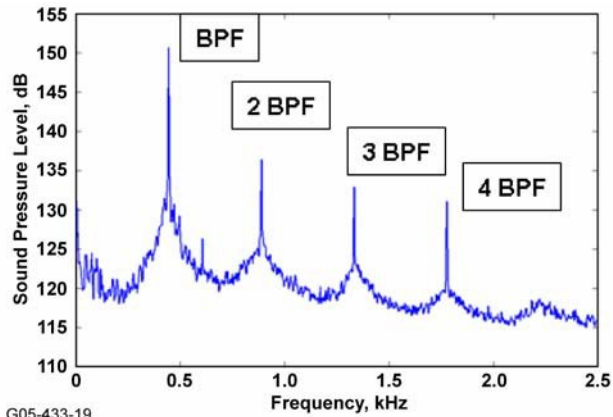
Figure 19.—Time domain Discrete Fourier Transform of windowed time history.
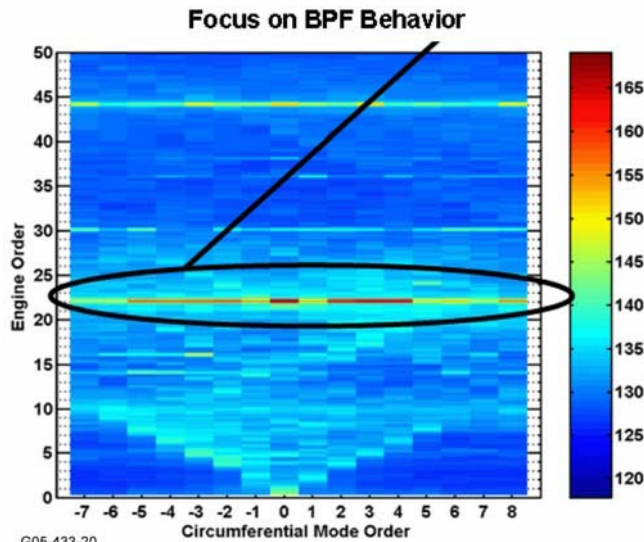
Figure 20.—Spatial domain modal amplitudes at all frequencies, focus on results at BPF or 22 engine orders (22EOs).
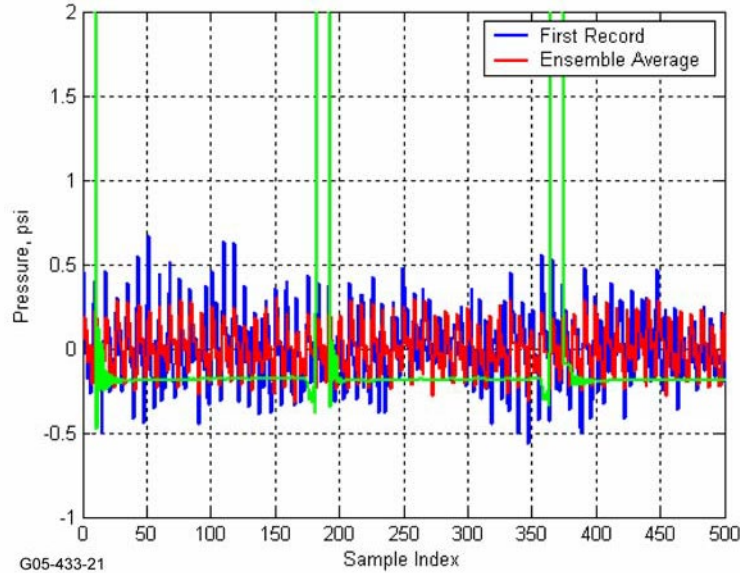
Figure 21.—Pressure time history with tach signal at the 352.5°
microphone position.

The conventional array method is expected to produce aliases of the fan and fan interaction modes due to the limited sensor count. The uniformly spaced 16 sensors will estimate unaliased spinning mode orders in the range of approximately –8 to 8 spinning mode orders. Table 1 contains the expected spinning mode orders using the classical Tyler-Sofrin relationship for the fan rotor and aft strut interactions for BPF and 2xBPF (n = 1 and n = 2) and Table 2 shows the expected aliased spinning modes for the 16 microphone uniform array at BPF (n = 1, from Table 1). The aliased modes are determined by the unaliased mode orders plus/minus and integer multiple of 16, the evenly spaced microphone count. The dark yellow in the tables indicates potential modes that may be cut-on in the duct based on an assumed duct Mach number, hub-to-tip ratio, and fan inlet temperature corresponding to a typical engine power setting representative of an approach-like condition. The number of propagating modes are increased as the Mach number is increased and as the temperature in the duct is reduced. The rotor/stator interactions are expected to be cut-off at the blade pass frequency (n = 1). The IGVs (19) also produce a number of interactions and corresponding aliases in the 16 microphone uniform array. The potential propagating modes resulting from the fan/IGV interaction are m = –54, –35, –16, 3, 22, and 41. There are many aliased modes in the 16 sensor array that result from the fan/IGV interaction; specifically, the m = 0 mode (resulting from the m = –16 fan/IGV interaction) that appears as one of the dominant modes in most of the modal results to follow.

TABLE 1.—FAN/STRUT (AFT) SPINNING MODE IDENTIFICATION

		B=Number of Blades =		22			V = Number of Strut Vanes =						10
		Mode = n*B + k*V												
		k=?												
		0	1	-1	2	-2	3	-3	-4	-5	-6	-7	-8	-9	-10	-11
n=?	1	22	32	12	42	2	52	-8	-18	-28	-38	-48	-58	-68	-78	-88
	2	44	54	34	64	24	74	14	4	-6	-16	-26	-36	-46	-56	-66

TABLE 2.—FAN/STRUT (AFT) MODES ALIASED
TO MODE ORDERS IN UNIFORM ARRAY

BPF Aliases for 16 Mic Uniform							
	3	2	1	0	-1	-2	-3
22	70	54	38	22	6	-10	-26
32	80	64	48	32	16	0	-16
12	60	44	28	12	-4	-20	-36
42	90	74	58	42	26	10	-6
2	50	34	18	2	-14	-30	-46
52	100	84	68	52	36	20	4
-8	40	24	8	-8	-24	-40	-56
-18	30	14	-2	-18	-34	-50	-66
-28	20	4	-12	-28	-44	-60	-76
-38	10	-6	-22	-38	-54	-70	-86
-48	0	-16	-32	-48	-64	-80	-96

3.4   Noise Measurement Testing and Test Matrix

Acoustic recordings are matched to the engine operating conditions, inlet AFC, and engine build configurations. Table 3 summarizes all the conditions at which acoustic data were acquired during the three engine builds of the VAIIPR noise program. In addition to the Build and Test identification, this table indicates the IGV setting, AFC setting, and the location on the performance map for each engine RPM setting. The nominal IGV settings for 63, 75 and 85 percent N_c, are 0°, 14°, and 12 °, respectively where the higher angle represents a higher degree of vane closing relative to the flow axis. Fan schedules and IGV settings (other than nominal) will be identified in the results and discussion sections pertaining to the IGV angle variation impact on noise. Active control settings were based on injection rate schedules and the injection location as determined by the VAIIPR program. Forward and aft refers to the location in the serpentine inlet. The forward position is just upstream of the initial bend closest to the inlet of the serpentine inlet. The aft position is just downstream of the final bend or turning location. The throttle settings indicated in the table correspond to different operating conditions along a given speed line. Details are provided in the discussion of results (see Section 4.0). There appears to be at least one sensor not functioning properly during all the builds and several conditions where more than one sensor was lost during the ~3 month duration of VAIIPR noise measurements. Additionally, there are some test conditions where the tachometer signal was not recorded or not functioning properly. These conditions are, for the most part, omitted from the detailed acoustic processing and evaluations in the following discussions.

TABLE 3.—VAIIPR ENGINE NOISE TEST RECORDINGS.

Build	Test Sequence	Test Run	RPM Nc	RPM % Nc	IGV Setting Degrees	Active Flow Control Setting Nominal	Max	Off	Fwd Only	Aft Only	Throttle Setting Speedline Location
4	32	1398	16177	85	Nominal	X					-7 Opline
4	32	1400	16177	85	Nominal	X					Nominal Opline
4	32	1402	16177	85	Nominal	X					Above Nominal Opline #1
4	32	1404	16177	85	Nominal			X			-7 Opline
4	32	1408	16177	85	Nominal			X			Nominal Opline
4	32	1414	16177	85	Nominal			X			Above Nominal Opline #1
4	32	1420	14274	75	Nominal	X					-7 Opline
4	33	1424	11990	63	Nominal	X					-7 Opline
4	33	1426	11990	63	Nominal	X					Nominal Opline
4	33	1428	11990	63	Nominal	X					Above Nominal Opline #2
4	33	1430	14274	75	Nominal	X					-7 Opline
4	33	1432	14274	75	Nominal	X					Nominal Opline
4	33	1434	14274	75	Nominal	X					Above Nominal Opline #1
5	86	4096	11990	63	Fan Schedule	X					-7 Opline
5	86	4100	11990	63	Fan Schedule	X					Above -7% Opline #2
5	86	4104	11990	63	Fan Schedule	X					Above Nominal Opline #1
5	87	4108	11990	63	Fan Schedule #1	X					-7% Opline
5	87	4112	11990	63	Fan Schedule #1	X					Above -7% Opline #2
5	87	4116	11990	63	Fan Schedule #1	X					Above Nominal Opline #1
5	88	4120	11990	63	Fan Schedule #2	X					-7% Opline
5	88	4124	11990	63	Fan Schedule #2	X					Nominal opline
5	88	4128	11990	63	Fan Schedule #2	X					Above Nominal Opline #2
5	90	4134	14274	75	Fan Schedule	X					-7% Opline
5	90	4140	14274	75	Fan Schedule	X					Nominal opline
5	90	4144	14274	75	Fan Schedule	X					Above Nominal Opline #2
5	91	4148	14274	75	Fan Schedule #1	X					-7% Opline
5	91	4145	14274	75	Fan Schedule #1	X					Nominal Opline
5	91	4158	14274	75	Fan Schedule #1	X					Above Nominal Opline #2
5	92	4162	14274	75	Fan Schedule #2	X					-7% Opline
5	92	4168	14274	75	Fan Schedule #2	X					Nominal opline
5	92	4172	14274	75	Fan Schedule #2	X					Above Nominal Opline #2
5	94	4178	16177	85	Fan Schedule	X					-7% Opline
5	94	4184	16177	85	Fan Schedule	X					Nominal Opline
5	94	4188	16177	85	Fan Schedule	X					Above Nominal Opline #2
5	95	4216	11990	63	Nominal	X					Below -7 Opline
5	95	4220	11990	63	Nominal	X					Above -7% Opline #1
5	95	4222	11990	63	Nominal	X					Nominal Opline
5	95	4228	11990	63	Nominal	X					Above Nominal Opline #3
5	96	4232	14274	75	Nominal	X					Below -7 Opline
5	96	4236	14274	75	Nominal	X					Above -7% Opline #1
5	96	4242	14274	75	Nominal	X					Above Nominal Opline #3
5	97	4246	16177	85	Nominal	X					Below -7 Opline
5	97	4250	16177	85	Nominal	X					Above -7% Opline #1
5	97	4254	16177	85	Nominal	X					Above Nominal Opline #1
5	98	4258	16177	85	Nominal		X				-7% Opline
5	98	4260	16177	85	Nominal		X				Above -7% Opline #1
5	98	4264	16177	85	Nominal		X				Above Nominal Opline #1
5	99	4268	16177	85	Nominal			X			Below -7 Opline
5	99	4272	16177	85	Nominal			X			Above -7% Opline #1
5	99	4278	16177	85	Nominal			X			Above Nominal Opline #3
5	100	4282	14274	75	Nominal			X			Below -7 Opline
5	100	4286	14274	75	Nominal			X			Above -7% Opline #1
5	100	4292	14274	75	Nominal			X			Above Nominal Opline #2
5	101	4296	11990	63	Nominal			X			Below -7 Opline
5	101	4302	11990	63	Nominal			X			Nominal Opline
5	101	4308	11990	63	Nominal			X			Above Nominal Opline #3
5	108	4345	16177	85	Nominal				X		Below -7 Opline
5	108	4349	16177	85	Nominal				X		Above -7% Opline #1
5	108	4353	16177	85	Nominal				X		Above Nominal Opline #1
5	109	4357	16177	85	Nominal					X	Below -7 Opline
5	109	4361	16177	85	Nominal					X	Below -7 Opline
5	109	4365	16177	85	Nominal					X	Above -7% Opline #1
5	120	4440	16177	85	Fan Schedule #1	X					-7% Opline
5	120	4446	16177	85	Fan Schedule #1	X					Nominal Opline
5	120	4450	16177	85	Fan Schedule #1	X					Above Nominal Opline #2
5	121	4454	16177	85	Fan Schedule #2	X					-7% Opline
5	121	4460	16177	85	Fan Schedule #2	X					Nominal Opline
5	121	4464	16177	85	Fan Schedule #2	X					Above Nominal Opline #2
6	139	4666	11990	63	epsilon = 0.0%	X					-7% Opline
6	139	4668	11990	63	epsilon = 2.4%	X					-7% Opline
6	141	4676	16177	85	epsilon = 0.0%	X					-7% Opline
6	142	4678	16177	85	epsilon = 1.9%	X					-7% Opline
6	142	4680	16177	85	epsilon = 3.0%	X					-7% Opline
6	143	4685	14274	75	epsilon = 0.0%	X					-7% Opline
6	145	4689	14274	75	epsilon = 3.3%	X					-7% Opline
6	146	4693	11990	63	epsilon = 2.3%	X					Above -7% Opline #1
6	146	4697	11990	63	epsilon = 2.5%	X					Nominal Opline

4.0   Measurement Results

4.1   General Observations

Data quality checks were performed on the measured pressure signals for each of the configurations identified in Table 3. Sensor sound pressure levels and sensor-to-sensor coherence were interrogated to identify unexpected trends in the data, faulty sensors, and the quality of the sound field in the duct at the frequencies of interest. Select results from this investigation of sensor performance are presented.

Sample output from "good channels" is shown in Figure 22 through Figure 24 from engine Build 4 at three different sensor locations in the circumferential array; 0°, 90°, and 270 °, respectively. These figures show the 63 percent N_c and 85 percent N_c results on the –7 percent engine operating line with the active control setting at its nominal position (AFC On). The blade pass tones and several multiples are clearly present in these figures, where BPF is just above 6000 Hz at 85 percent speed and near 4500 Hz at 60 percent speed. At 85 percent N_c, a few shaft harmonics appear likely due to multiple pure tone noise where the blade tips may be supersonic. The acoustic levels are representative of typical inlet noise levels for this fan. In contrast, the sensor at the 180° position in the circumferential array at 63 percent N_c showed very high broadband noise levels relative to the rest of the sensors in the array during Build 4 data acquisition. Output from this sensor is shown in Figure 25, which is characteristic of its output throughout all Build 4 noise testing. A similar result was observed from the 0° sensor as well as the 180° sensor during all of Build 5 testing. In addition, other sensors failed during different configurations of Build 5 testing. Sensor performance at the 22.5°, 37.5°, and 240 ° locations was deemed unacceptable during all of Build 6 noise testing.

Figure 26 and Figure 27 show the data at two different engine speeds for the 12 o'clock and 6 o'clock sensors at the inlet of the serpentine inlet, respectively (see Figure 12) for the engine operating speeds 63 percent N_c and 85 percent N_c on the –7 percent operating line with the active control setting at its nominal position (AFC On). These figures show the blade pass tone and several harmonics similar to the data from the 32-sensor array near the fan inlet but at much lower levels. As might be expected, the inlet duct appears to provide significant attenuation of noise propagating from the fan, comparing Figure 22 through Figure 24.
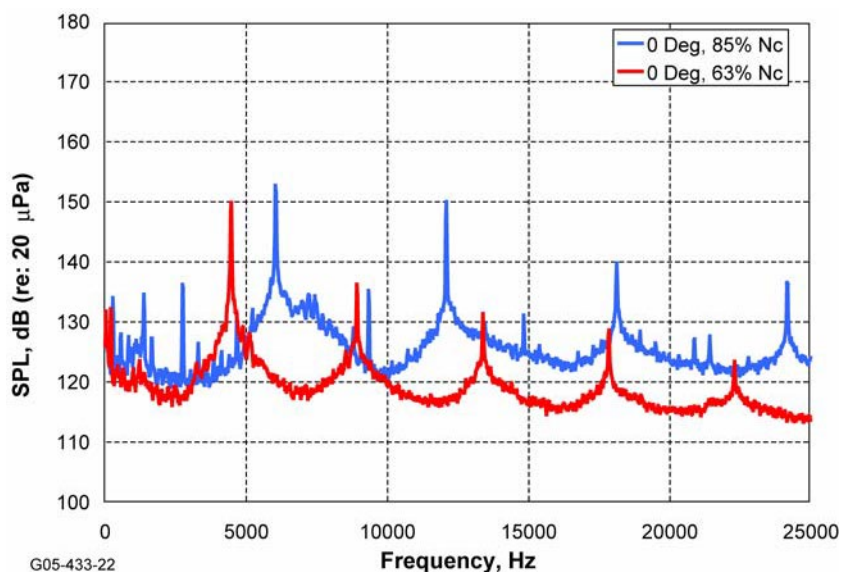

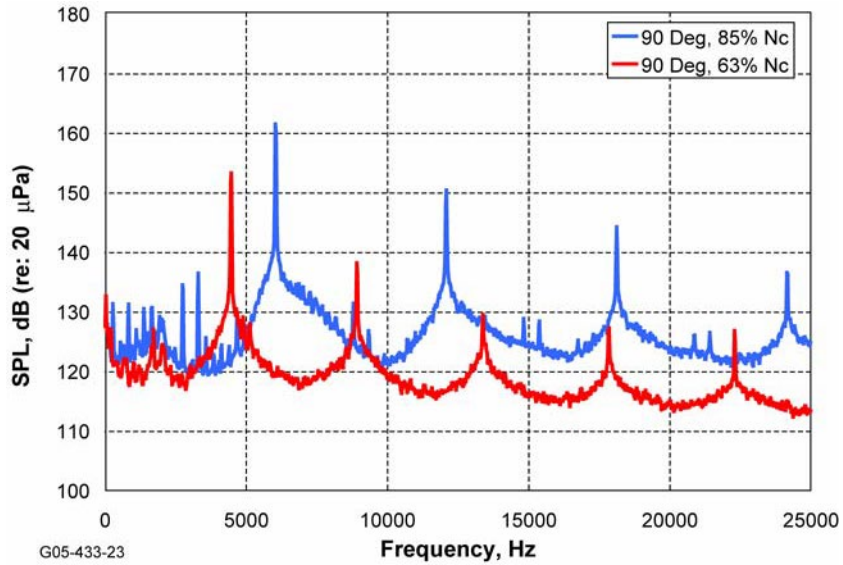Figure 22.—Build 4 engine test data at the 0° sensor location.

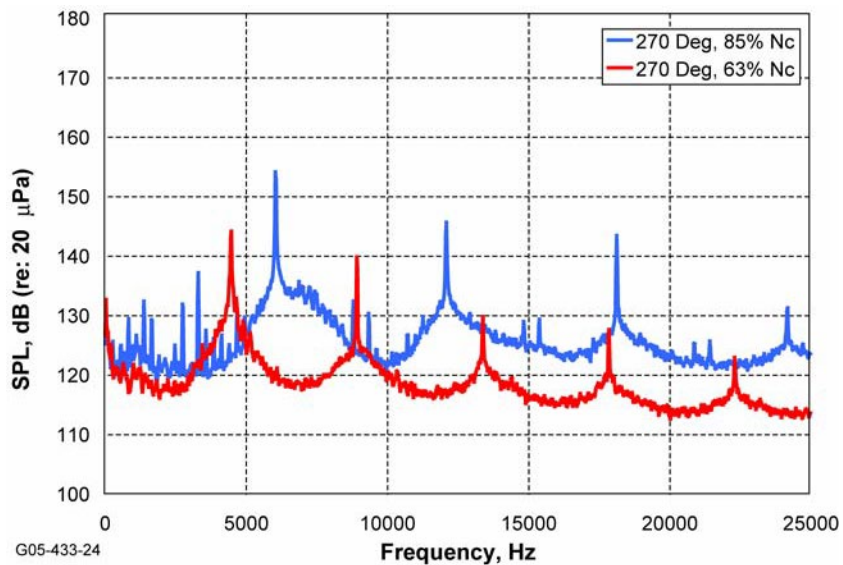Figure 23.—Build 4 engine test data at the 90° sensor location.

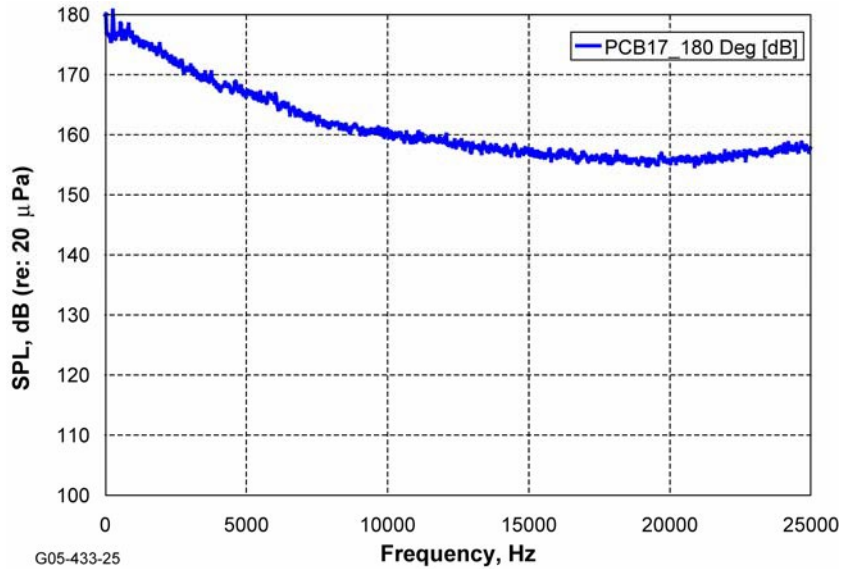Figure 24.—Build 4 engine test data at the 270° sensor location.

Figure 25.—Build 4 engine test data at the 180° sensor location for 63 percent N_c.
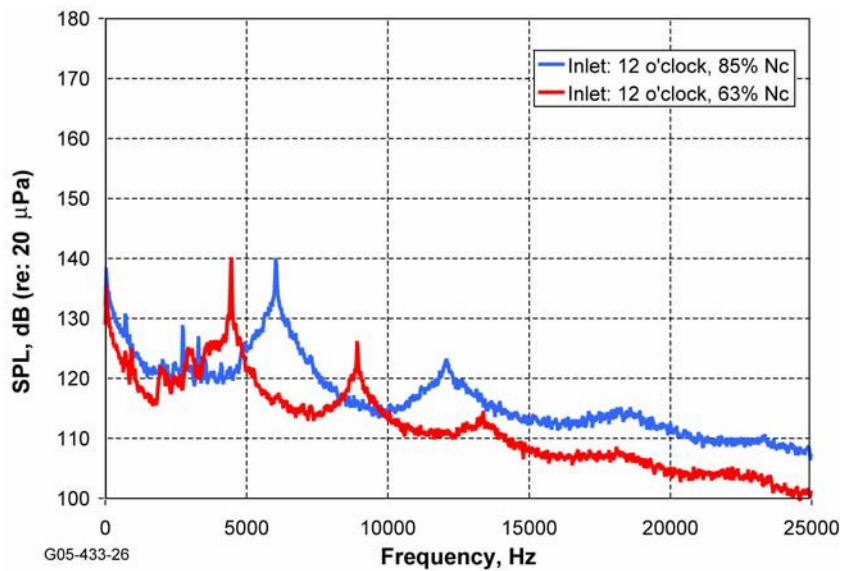

Figure 26.—Build 4 engine test data at the inlet 12 o'clock or 0° sensor location.
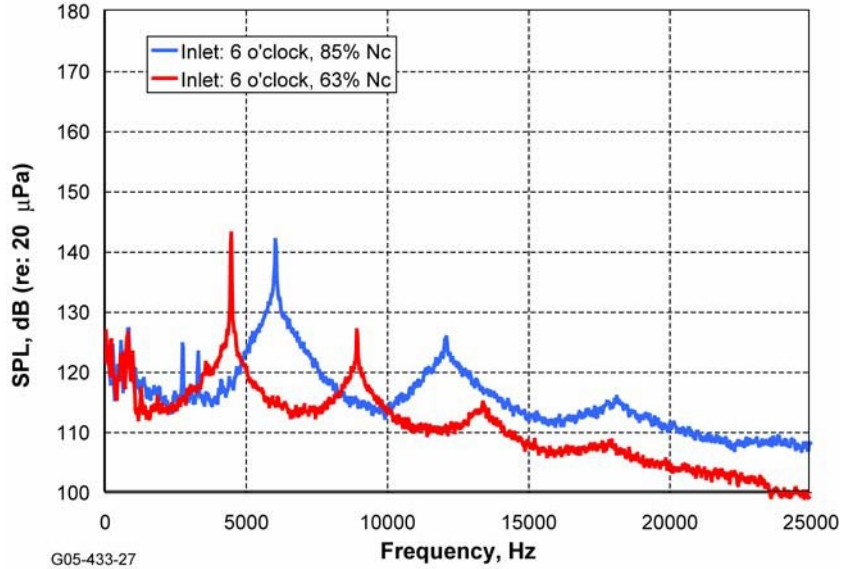
Figure 27.—Build 4 engine test data at the inlet 6 o'clock or 180° sensor location.

For a single sound source in an infinite duct with no internally reflecting surfaces, the coherence between sensors should be unity (Ref. 13). In an engine duct with both rotating and stationary engine components there may be multiple uncorrelated broadband and tone noise sources as well as many reflecting surfaces. With that said, it is still expected that the coherence should be high at the blade pass frequency and its harmonics and essentially unity when the time domain coherent processing is applied as previously described.

The ordinary coherence function is defined as follows;

$$\gamma^2 = \frac{\left|G_{xy}(f)\right|^2}{G_{xx}(f) \cdot G_{yy}(f)}$$

Where G_{xy} is the cross power spectrum between microphone signals x and y, G_{xx} is the autospectrum of microphone x, and G_{yy} is the autospectrum of microphone y. The plots to follow show the coherence between all 32 sensor pairs [32 x 32] in the circumferential array near the fan. The diagonal elements should be perfectly coherent and will appear red (dark) along the diagonal of the plots to follow. Also, the coherence plots are symmetric about the diagonal ($G_{xy} = G_{yx}$).

Figure 28 and Figure 29 show the coherence levels between microphone sensors at BPF for the 63 percent N_c speed setting on the nominal op-line with AFC off and AFC on, respectively. Figure 30 and Figure 31show the coherence levels between microphone sensors at 2xBPF for the 63 percent N_c speed setting on the nominal op-line with AFC off and AFC on, respectively. At BPF for this engine configuration, the sensor-to-sensor coherence levels are all relatively high except sensor 1 and 23 with all other sensors. The coherence levels are improved at essentially all combinations for the condition of AFC on. At 2xBPF, the coherence levels are much lower, with again an improvement with AFC on. As expected, the time domain ensemble averaging (using the 1/rev signal) resulted in nearly perfect coherence between all sensors at BPF and harmonics. Color maps similar to the previous coherence results would be completely red (dark) for all sensor pairs and are therefore omitted. These results suggest that there may be random sources (as might be expected of the complex internal system) in the duct that are not shaft dependent.
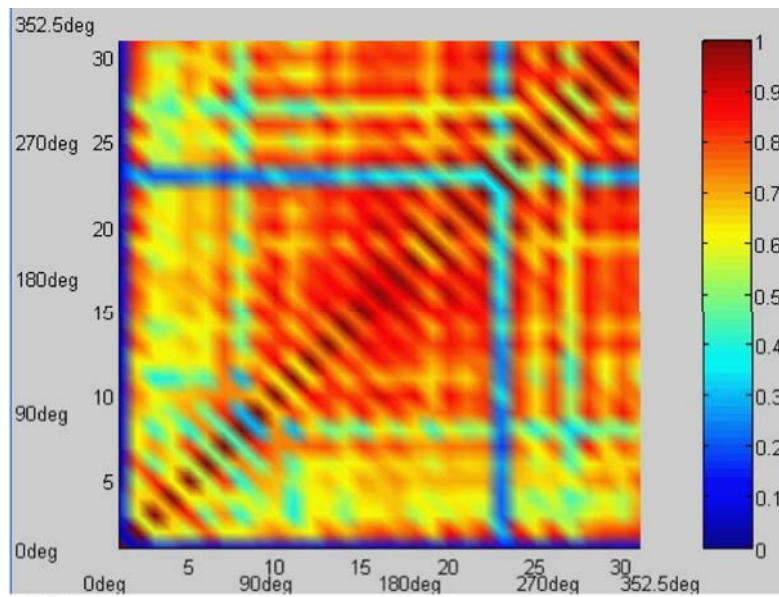
Figure 28.—Sensor-to-sensor coherence at BPF for the 63 percent N_c speed setting on the nominal op-line with AFC off.
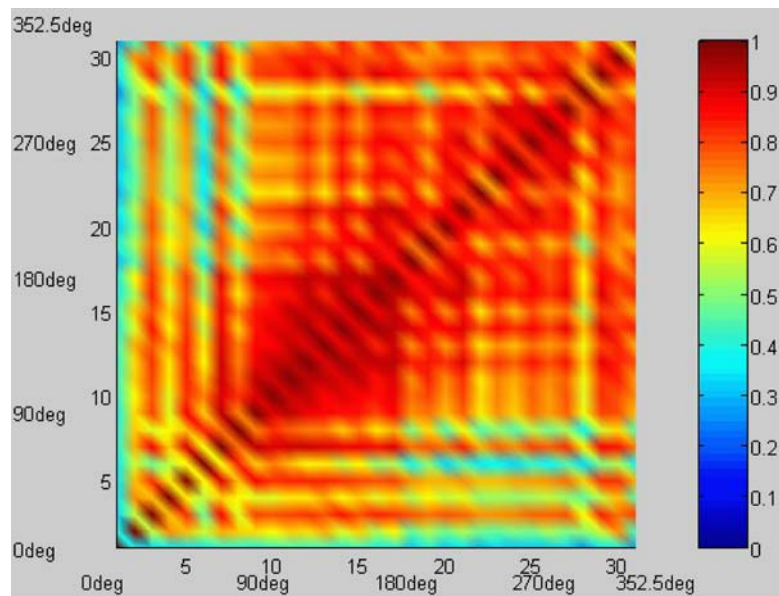
Figure 29.—Sensor-to-sensor coherence at BPF for the 63 percent N_c speed setting on the nominal op-line with AFC on.
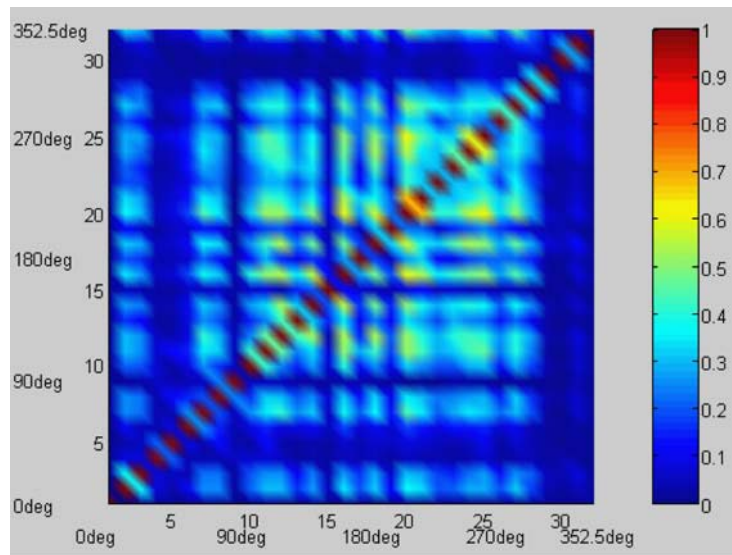
Figure 30.—Sensor-to-sensor coherence at 2xBPF for the 63 percent N_c speed setting on the nominal op-line with AFC off.
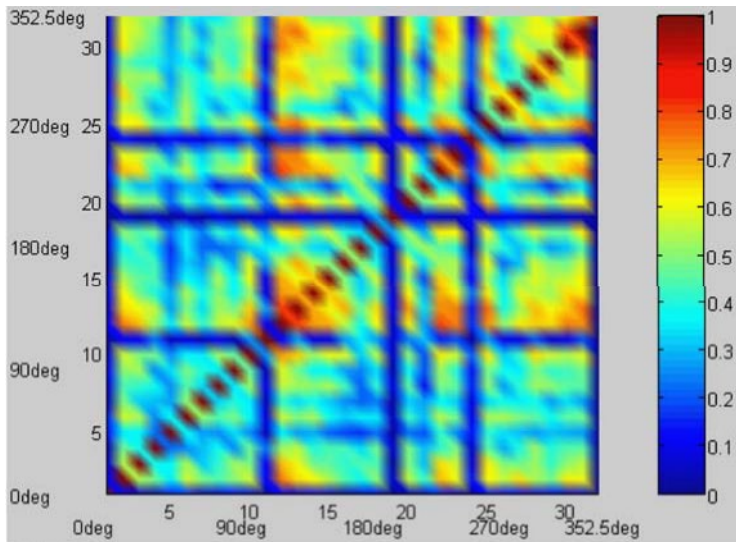
Figure 31.—Sensor-to-sensor coherence at 2xBPF for the 63 percent N_c speed setting on the nominal op-line with AFC off.

4.2   Interaction Modes and Mode Aliases

Potential interaction modes and the aliases from these modes for the 16-sensor evenly spaced array are identified and Table 4 and Table 5, respectively. The interaction modes are calculated based on the previously defined Tyler-Sofrin relationship and are consistent with the results shown in Table 1 and Table 2.

TABLE 4.—POTENTIAL CUT-ON INTERACTION MODES AT BPF

Fan/	Potential Cut-On Interaction Modes								
IGV's	41	3	−16	−35	−54				
Stator	−30								
Struts	52	42	32	12	2	−8	−18	−28	−38	−48

TABLE 5.—ALIASED MODES FROM INTERACTIONS
AT BPF FOR 16-SENSOR EVENLY SPACED ARRAY

| Fan/	Aliased Modes in 16-Sensor Evenly Spaced Array								
IGV's	−7	3	0	−3	−6				
Stator	2								
Struts	4	−6	0	−4	2	8	−2	4	−6	0

4.3   Changes in Inlet Distortion Due to Active Flow Control

Figure 32 shows the serpentine inlet with the approximate locations of the active flow control air supply in the duct. The forward (AFC Fwd) and aft introduction (AFC Aft) of flow control is identified. The AFC On condition (indicated in the discussions to follow) represents the condition with the addition of both forward and aft flow control. The details of this device and its specific application during VAIIPR testing are deliberately left out for proprietary reasons.

An examination of the narrowband pressure spectra as an average the circumferential array of p^2 values is shown in Figure 33 representing a typical approach condition, 63 percent N_c. This figure clearly shows that the broadband noise was reduced when the AFC was turned on (both Fwd and Aft operating at the nominal setting) indicating that the AFC may reduce the overall turbulence level in the inflow due to the improvement in flow quality. However, the blade pass tone was slightly increased and the 2xBPF tone and other integer harmonics are significantly increased as seen in Figure 33. Figure 34 shows the effect of AFC On versus Off at the same engine conditions summarizing the differences in terms of an overall (all positions/all frequencies) p^2 level and the circumferentially averaged level at BPF and 2xBPF.
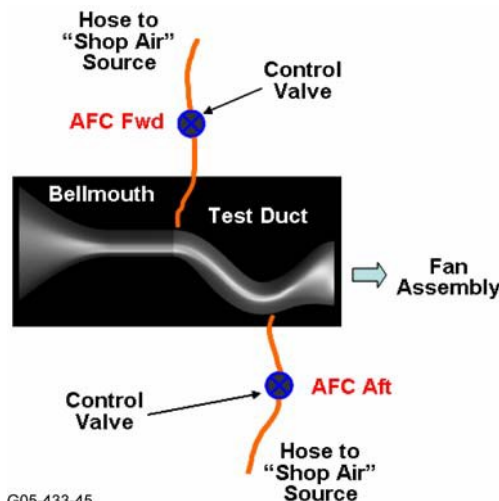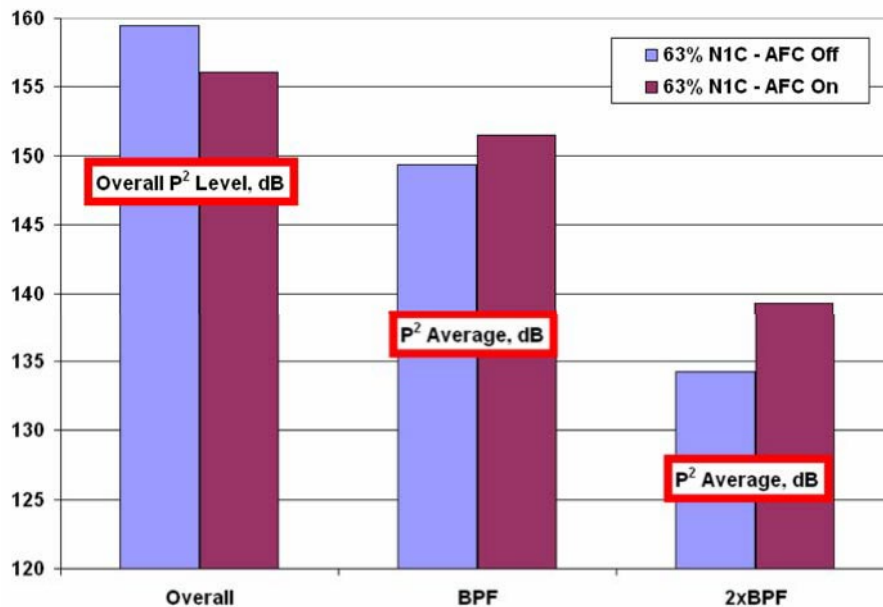

Figure 32.—Schematic of active flow control
device with the serpentine inlet duct.
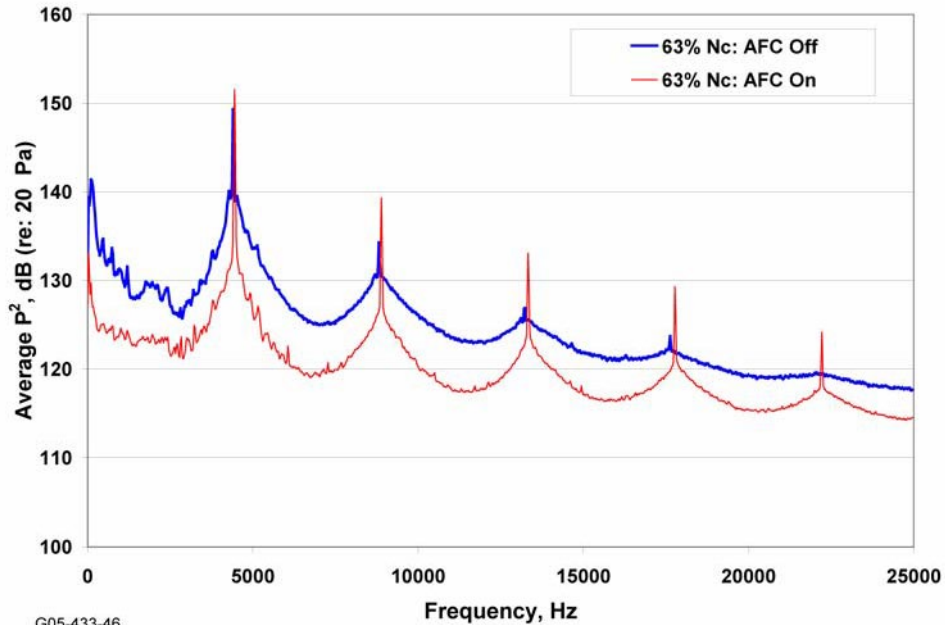
Figure 33.—The effect of AFC on the circumferentially averaged P^2 levels from the 32-sensor array for 63 percent N_c (below –7 percent op-line).

Figure 34.—The effect of AFC on the circumferentially averaged P^2 levels from the 32-sensor array for 63 percent N_c (below –7 percent op-line): overall, BPF and 2xBPF.

Figure 35 and Figure 36 show similar results again at 63 percent N_c but on the nominal engine op-line. The slight noise increase at BPF for the nominal op-line (blue line in Figure 35) compared to below the –7 percent below the nominal op-line (blue line in Figure 33) might be expected due to the slightly higher fan pressure ratio and slightly higher tip Mach numbers for the same speed setting. These sets of figures and different op-lines, are consistent in that both indicate a slight decrease in the overall p^2 level with the introduction of AFC, and a no to slight increase in averaged p^2 level at BPF and 2xBPF.
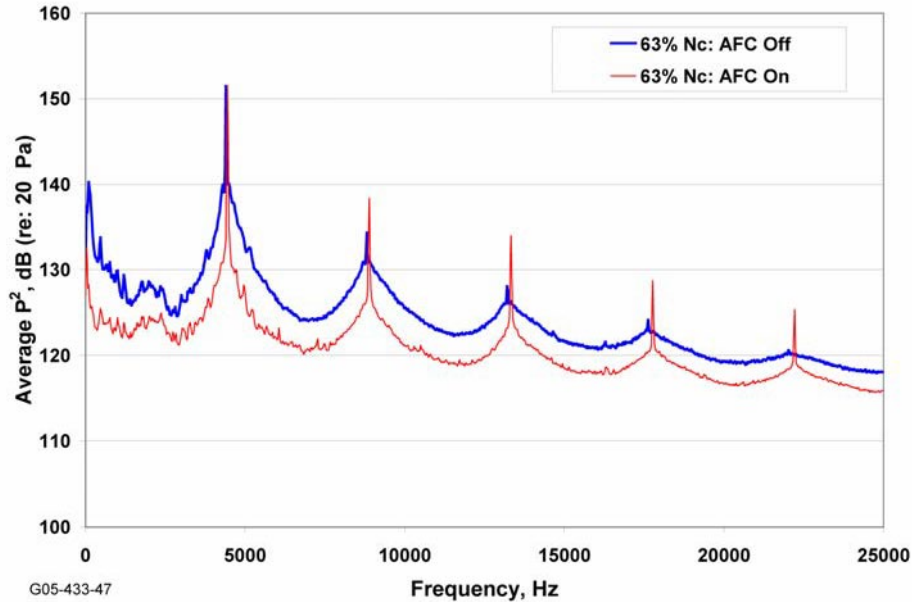
Figure 35.—The effect of AFC on the circumferentially averaged P^2 levels from the 32-sensor array for 63 percent N_c (nominal op-line).
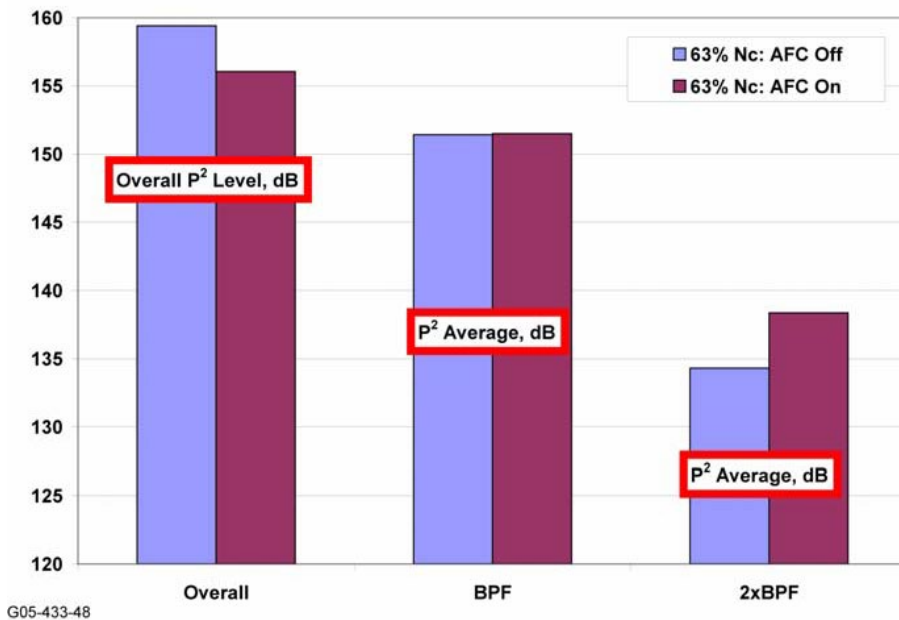
Figure 36.—The effect of AFC on the circumferentially averaged P^2 levels from the 32-sensor array for 63 percent N_c (nominal op-line): overall, BPF and 2xBPF.

Modal data from the uniform array for the 63 percent N_c engine operating condition (nominal op-line) without AFC and with AFC on are shown in Figure 37. These results indicate the presence of a strong $m = 0$ mode at the blade pass frequency for both conditions. This mode may be an aliased spinning mode from both the fan/strut as well as the fan/IGVs, refer to mode and mode aliases listed in Table 4 and Table 5, respectively. The $m = 2$ and $m = 4$ modes can be attributed to identifiable interactions in the duct. Also, $m = 3$ more pronounced in the AFC On condition may be attributed to the fan/IGV interaction. The ±1 spinning modes do not appear to be a combination or alias of any of the potential cut-on interactions. The
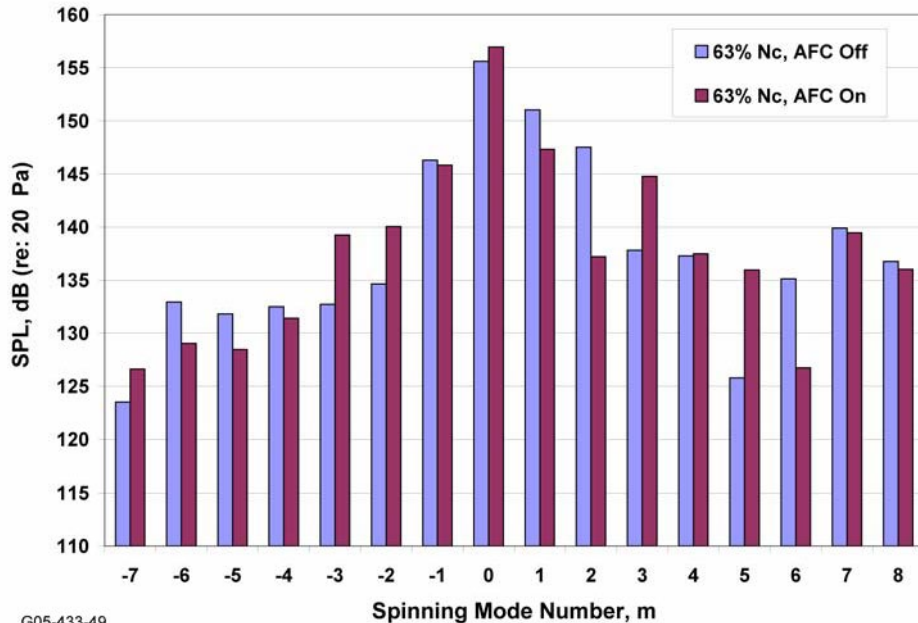
Figure 37.—Spinning mode content for 63 percent N_c (nominal op-line) with AFC off and AFC on.

$m = 6$ mode appears to quite low. This mode is the alias of the $m = 22$ rotor alone mode and is not expected to be a big contributor to the modal energy until higher engine speed settings. The overall performance of the active flow control (cleaner inflow) appears to have reduced the modal amplitudes of most modes in the duct with a slight increase in the $m = 0$ mode consistent with the spatially average narrowband results. It is also worth noting that a 1/rev distortion, natural distortion pattern from a serpentine inlet, could potentially generate interaction modes at all integers substituting $V = 1$ in the Tyler-Sofrin relation.

With 31 of the 32 sensors available in the circumferential array for this test case, the Virtual Array was used and appears to have adequately identified this fan/IGV interaction as the aliased $m = 0$ mode in the 16 sensor evenly spaced array results. Figure 38 shows the results from the Virtual Array with the $m = -16$ spinning mode dominant. Sidelobes at $m = 0$ and $m = 16$ are also somewhat present and may be due to aliasing effects with the reduced Virtual Array sensor count. It should be noted that the Virtual Array concept was developed primarily to identify spinning mode content; hence potential interaction modes for identifying noise sources. The Virtual Array subspace method (as formulated) does not rely on amplitude readouts given that the problem is formulated on the basis of a referenced sensor point, sensor 1, and the amplitude is relative to this reference point which does not reflect the actual magnitude. As a result, the Virtual Array data are presented in a normalized manner. Coupled with the results of the evenly spaced array, it appears that the fan/IGV interaction is a dominant interaction for this engine configuration.

Corresponding distortion data from aerodynamic interface plane (AIP) rakes shows the impact of active flow control on the flow into the fan duct, see Figure 39 and Figure 40. These figures show the 180° position as the 12 o'clock position or top-dead center (TDC). Comparing these figures, the stationary inlet distortion patterns for the conditions of active flow control off and on, clearly indicate the removal of the low-pressure 1-per-rev distortion with the addition of active flow control. The circumferential distortion index (CDI) for active flow control off is 0.01979 and for active flow control on is 0.00705 corresponding to Figure 39 and Figure 40, respectively. The coherent portion of the noise data (BPF and multiples of BPF) was not reduced with the introduction of AFC and did not positively correlate with the observed reduction in circumferential distortion as might be expected.
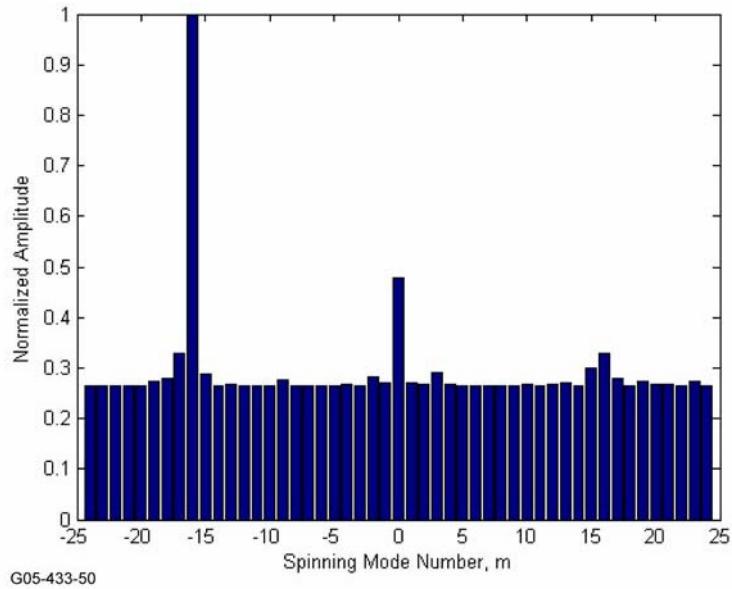
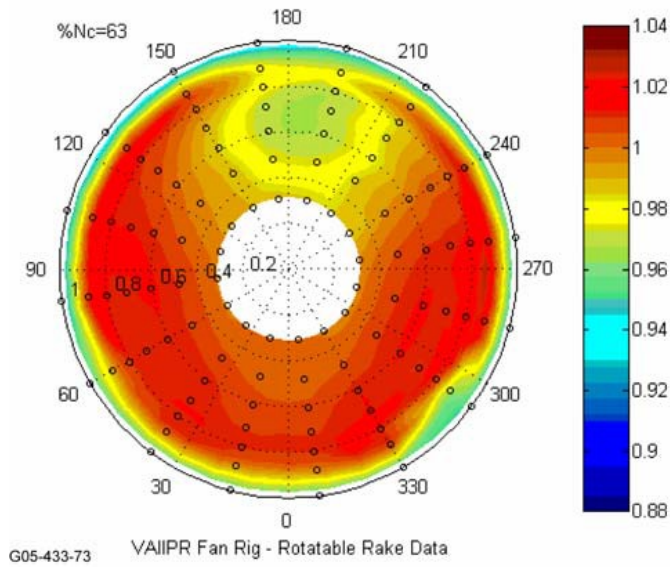Figure 38.—Virtual array results for 63 percent N_c (nominal op-line) with AFC off.

G05-433-73   VAIIPR Fan Rig - Rotatable Rake Data

Figure 39.—Total pressure contour for 63 percent N_c (nominal op-line) with AFC off.
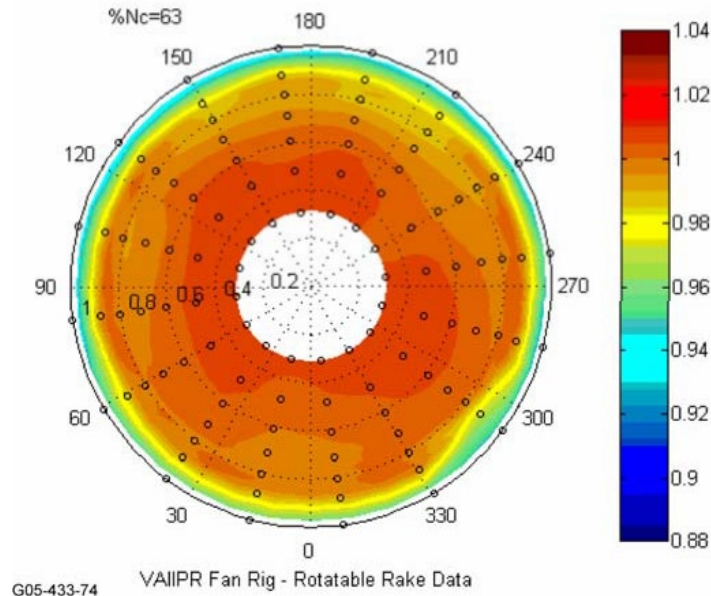
Figure 40.—Total pressure contour for 63 percent N_c (nominal op-line) with AFC off.

The modal decomposition, from the uniformly spaced array of 16 sensors, for 2*BPF is shown in Figure 41 and Figure 42 for active flow control on and off, respectively. The modal behavior at 2*BPF also appears to be consistent with the averaged p^2 behavior seen previously in Figure 35 and Figure 36 where now the active flow control off condition is significantly lower in averaged SPL as are the modal amplitudes significantly lower compared to AFC on. As indicate in Figure 36, the amplitudes at both active flow conditions at 2*BPF are significantly less than the BPF condition. The m = –3 mode is also (m = 0 at BPF) an aliased mode from the interaction of the fan with the IGVs at 2*BPF.

Figure 43 shows a comparison of the narrowband pressure spectrum for the circumferentially averaged pressure with the AFC on and off for a typical cutback takeoff condition, 75 percent N_c. The AFC slightly reduced the blade pass tone and broadband noise levels. The higher blade pass tone harmonics were increased with the introduction of the AFC. Figure 44 shows the results of the total averaged p^2 level in the inlet near the fan at a typical cutback takeoff condition based on the noise spectrum in Figure 43. Again (as with the approach condition), it can be seen from the results that the AFC reduced the overall p^2 level in the inlet duct. In addition, the blade pass tone power was slightly reduced for this condition and the twice blade passage frequency was increased by the AFC. Figure 45 and Figure 46 show similar results and trends for the 75 percent N_c case at a slightly higher pressure ratio and lower inlet flow condition (above – 7 percent op-line). Again, the broadband levels are reduced with a slight decrease at BPF and an increase at 2*BPF.
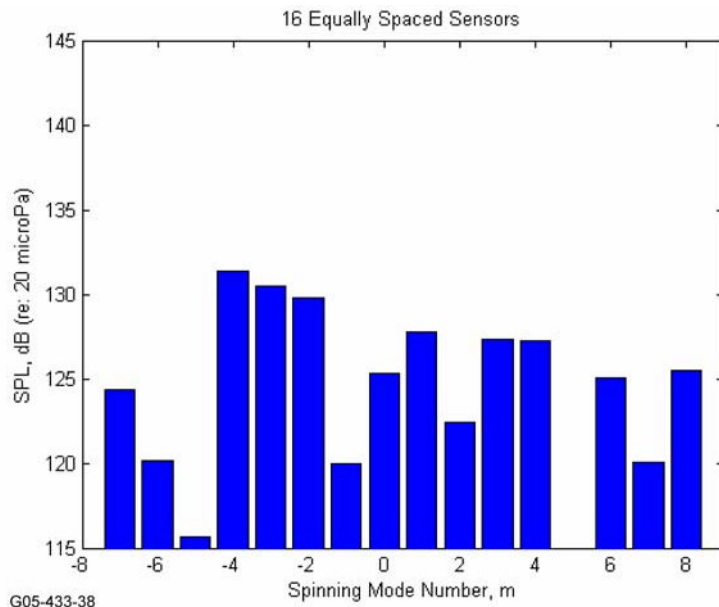
Figure 41.—Spinning mode content at 2*BPF from uniformly spaced array for 63 percent N_c (nominal op-line) with AFC off.
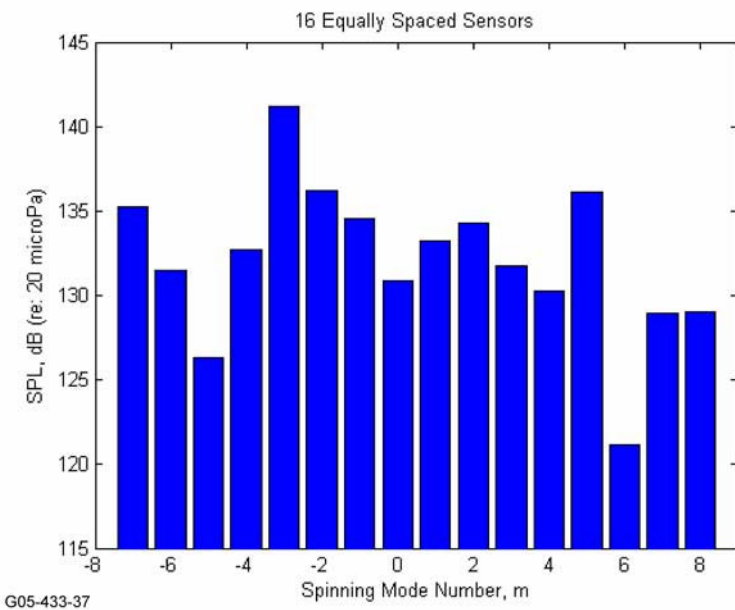
Figure 42.—Spinning mode content at 2*BPF from uniformly spaced array for 63 percent N_c (nominal op-line) with AFC on.
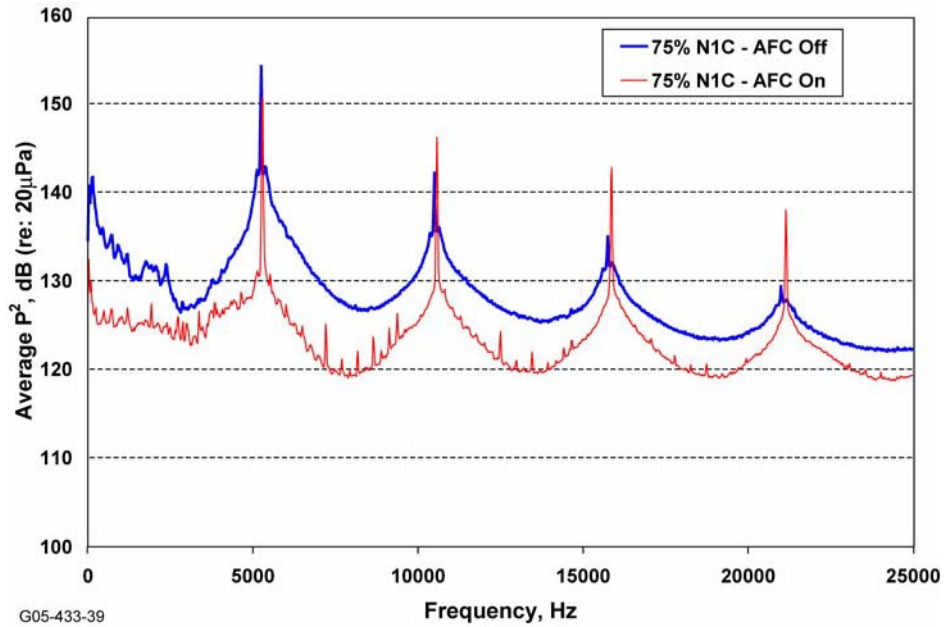
G05-433-39

Figure 43.—The effect of AFC on the circumferentially averaged P^2 levels from the 32-sensor array at 75 percent N_c (below –7 percent op-line).
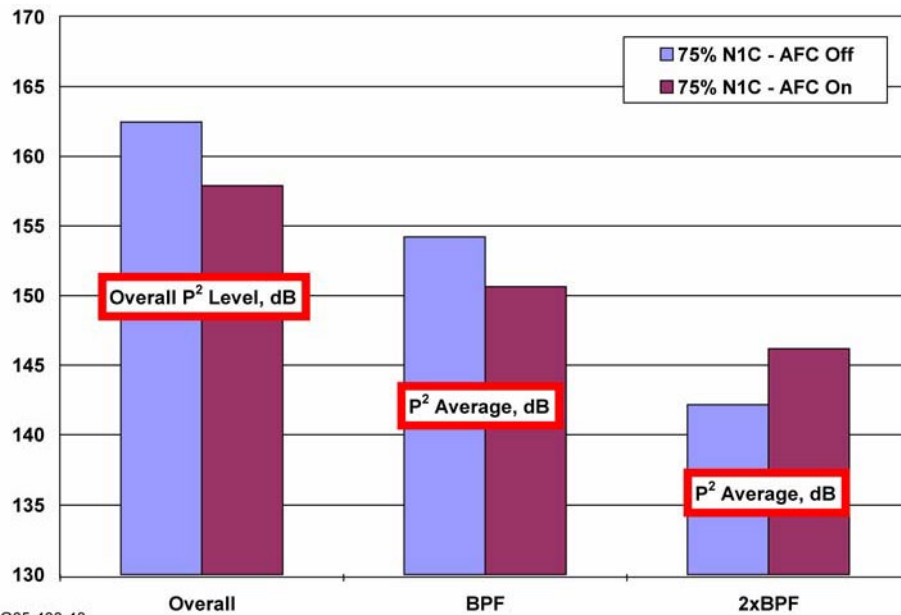
G05-433-40

Figure 44.—The effect of AFC on the circumferentially averaged P^2 levels from the 32-sensor array at 75 percent N_c (below –7 percent op-line): overall, BPF and 2xBPF.
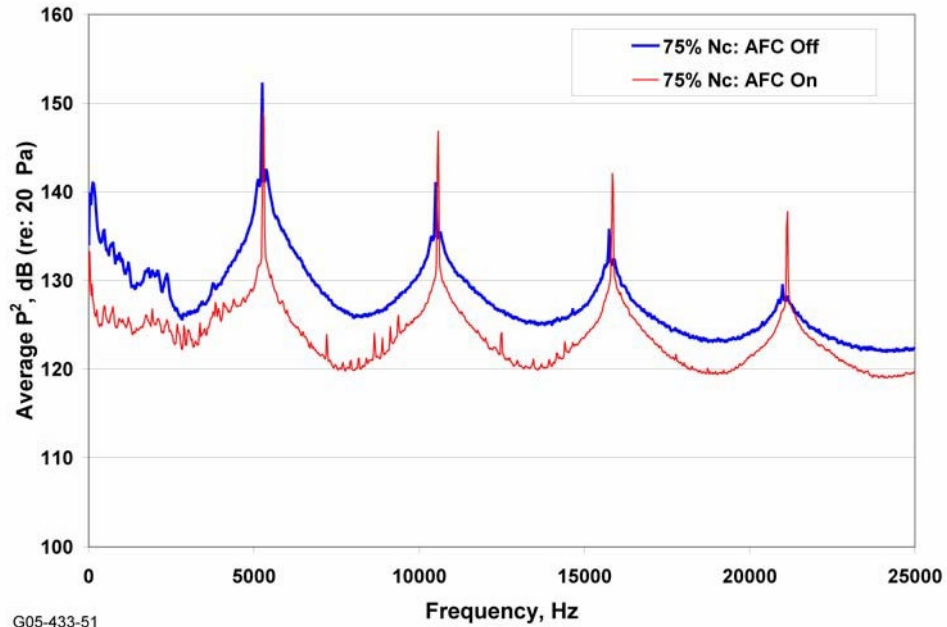
Figure 45.—The effect of AFC on the circumferentially averaged P^2 levels from the 32-sensor array at 75 percent N_c (above –7 percent op-line).

Figure 46.—The effect of AFC on the circumferentially averaged P^2 Levels from the 32-sensor array at 75 percent N_c (above –7 percent op-line): overall, BPF and 2xBPF.

Modal data from the uniform array for the 75 percent N_c engine operating condition (above –7 percent op-line) with AFC off and on are shown in Figure 47. These results indicate a weaker presence of m = 0 mode at the blade pass frequency for both conditions. The m = 3 mode is more prominent in this dat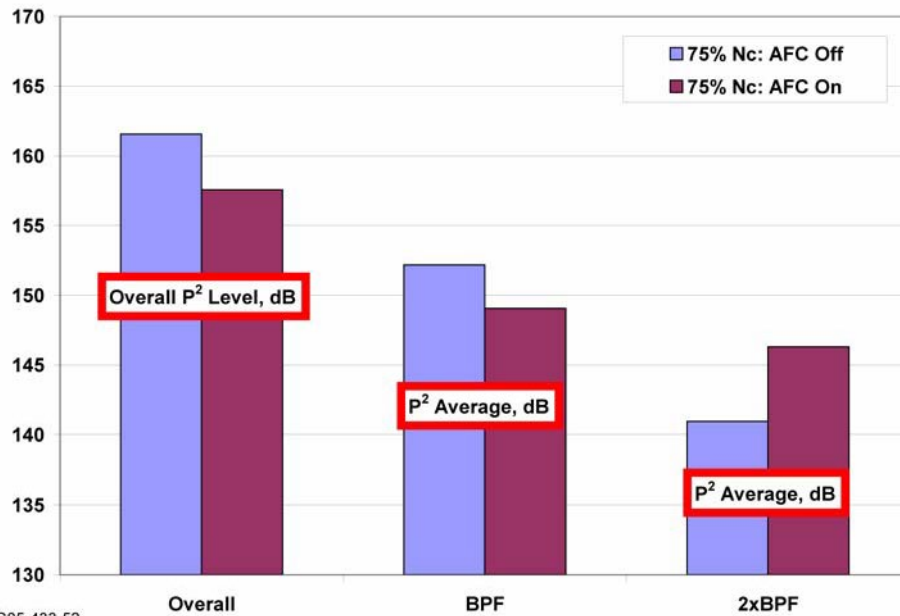a, this mode has already been identified as an interaction from the fan/IGVs. The strong m = 4 could be the result of the fan interacting with the aft struts. The m = 6 mode is also a little more energized at this condition. This mode is the alias of the m = 22 rotor alone mode and is not expected to be a big contributor to the modal energy until higher engine speed settings. For this condition, active flow control has reduced the modal energy from key fan interactions resulting in slightly lower in-duct noise levels near the fan face at the BPF tone with active flow control. These modal results are also consistent with the spatially averaged narrowband noise results.

The data show a slightly different impact of the AFC at a typical full power takeoff condition, 85 percent N_c. The narrowband data in Figure 48 show a significant decrease in broadband noise levels consistent with the other engine speed settings but a gradual increase in the BPF tone and 2*BPF with the introduction of active flow control. Figure 49 shows that the overall mean square pressure levels remained relatively unchanged with the introduction of the AFC. This increase in tone levels is roughly balanced by the decrease in broadband levels. However, the levels at the blade pass and twice blade pass tones increased. Active flow control is introduced incrementally. Broadband levels are only slightly reduced with AFC Aft and dramatically reduced with AFC On. Figure 50 and Figure 51 show similar results and trends for the 85 percent N_c case at a slightly higher pressure ratio and lower inlet flow condition (above –7 percent op-line). These figures have an additional AFC condition, AFC Max, where the flow rates from the active flow control devices were increased somewhat from the nominal AFC On setting. Little to no difference is observed in the noise data between these two conditions.
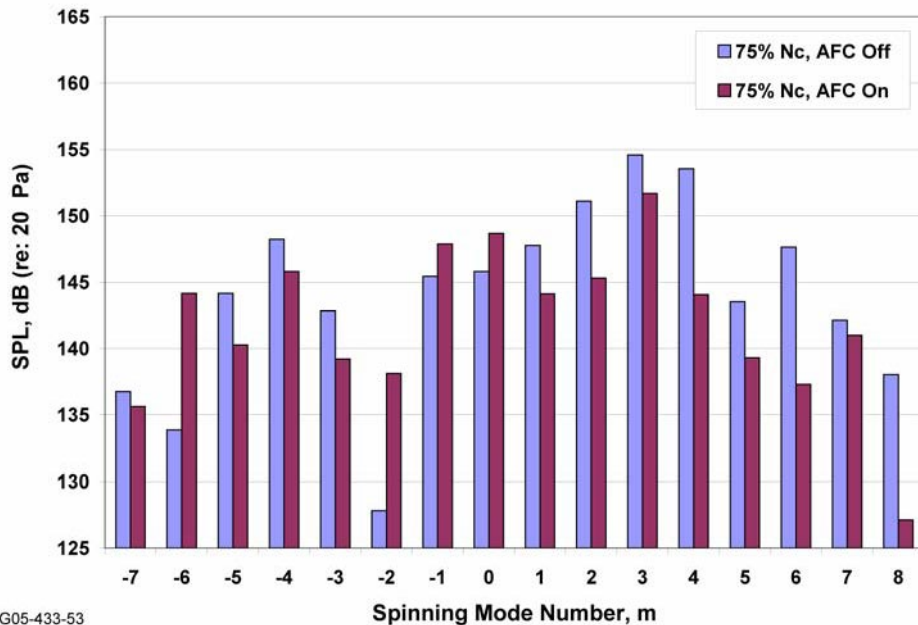
Figure 47.—Spinning mode content for 75 percent N_c (above –7 percent op-line) with AFC off and AFC on.

Figure 48.—The effect of AFC on the circumferentially averaged P^2 levels from the 32-sensor array at 85 percent N_c (below –7 percent op-line).

Figure 49.—The effect of AFC on the circumferentially averaged P^2 levels from the 32-sensor array at 75 percent N_c (below –7 percent op-line): overall, BPF and 2xBPF.

Figure 50.—The effect of AFC on the circumferentially averaged P^2 levels from the 32-sensor array at 85 percent N_c (above –7 percent op-line).
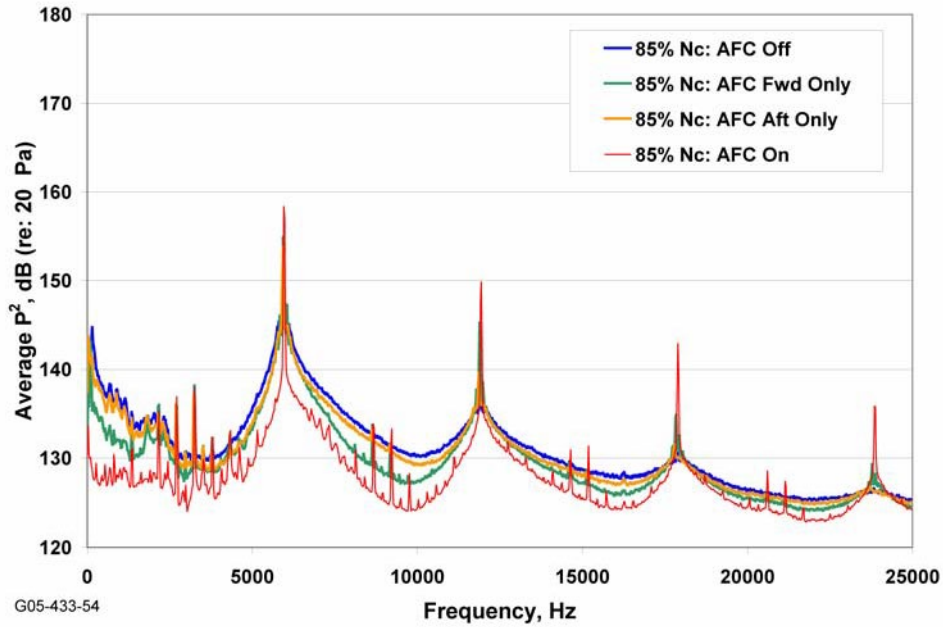

Figure 51.—The effect of AFC on the circumferentially averaged P^2 levels from the 32-sensor array at 85 percent N_c (above –7 percent op-line): overall, BPF and 2xBPF.
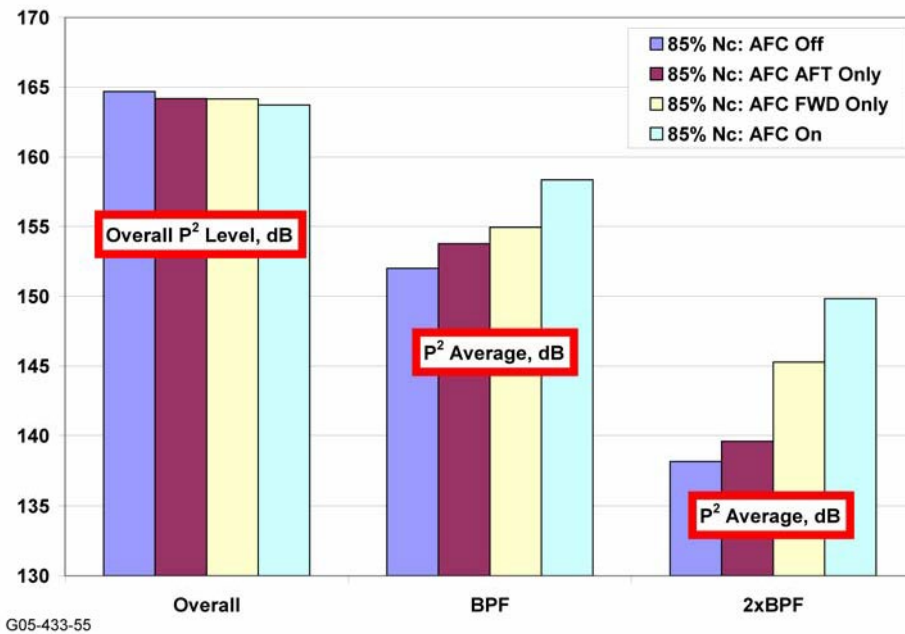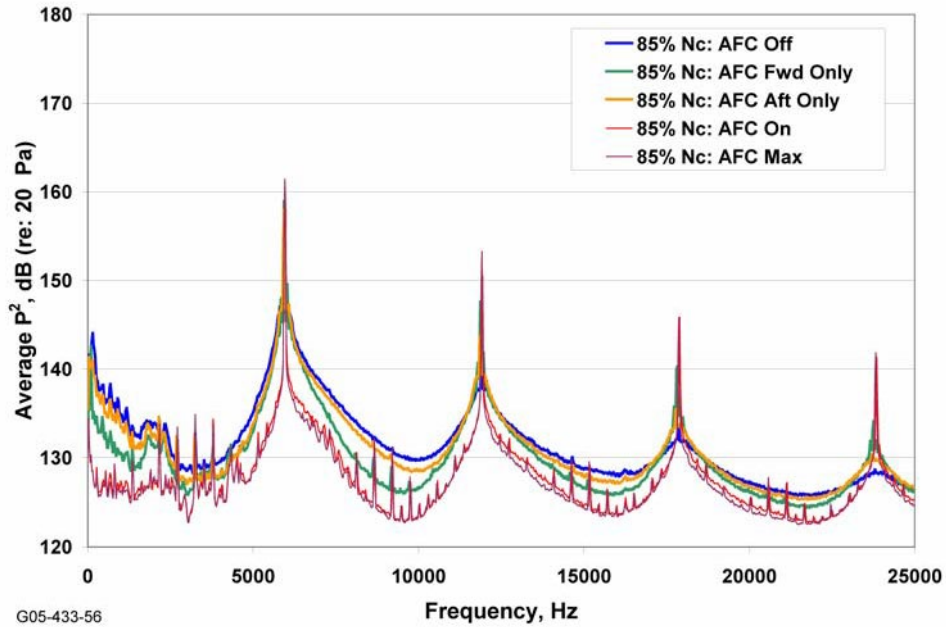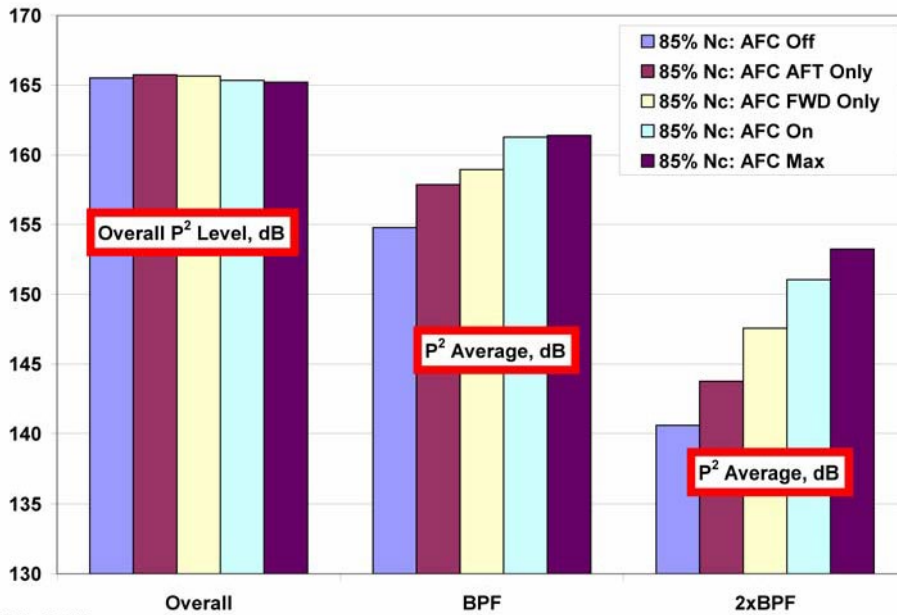
Modal decomposition results using the 16 sensor evenly spaced array are presented in Figure 52 through Figure 54 for AFC off, AFC fwd, and AFC on, respectively. These results correspond to the noise data and engine condition contained in Figure 50 at the blade pass tone. The modal plots show the presence of the m = 6 mode for the AFC On condition which is an aliased mode of the m = 22 fan mode. This rotor alone mode may be expected due to higher blade tip Mach numbers. The rotor alone mode amplitude is reduced with AFC. It appears the overall broadband modal energy is increased with the addition of active flow control, a result that contradicts the spatially averaged spectra and the behavior at other speeds.

Figure 53 show the results from the Virtual Array for the 85 percent N_c speed condition similar to that in Figure 52. The m = 22 spinning mode is a dominant mode and may be attributed to the rotor potential field associated with this higher speed condition. It should be noted that 2 of the 32 sensors in the Virtual Array were disregarded from the processing due to poor signal quality. The Virtual Array has adequately identified the rotor alone mode identified as the aliased m = 6 mode in the 16 sensor evenly spaced array results. There appears to be some significant energy in the m = 21 and m = 23 modes surrounding the m = 22 mode in addition to the potential presence of an m = 17 modes. These modes do not correspond to the interactions identified in Table 4; however, the m = 21 and m = 23 modes were also identified in previous modal testing of a similar TFE731-60 fan assembly, see Figure 1.

G05-433-58
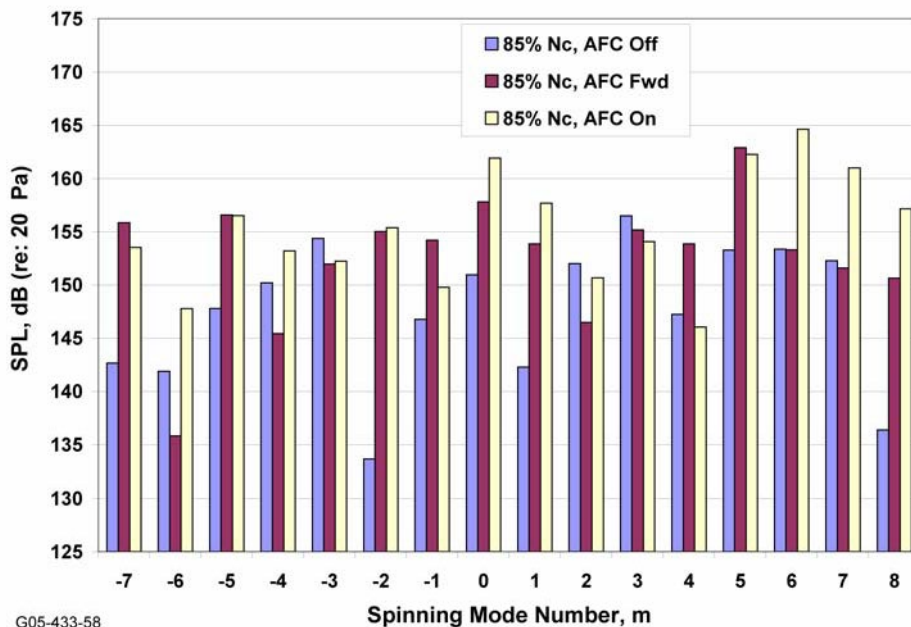
Figure 52.—Spinning mode content at 85 percent N_c (above –7 percent op-line) for AFC off.
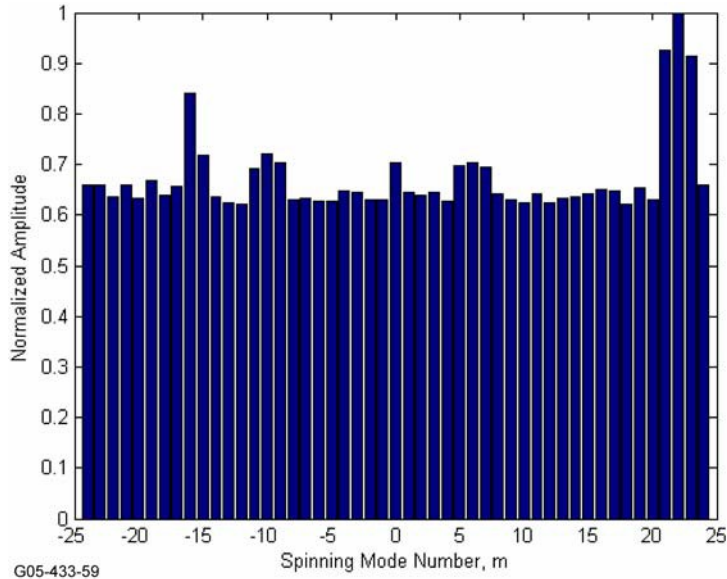
Figure 53.—Virtual array results for 85 percent N_c (above –7 percent op-line) engine operating condition with AFC off.
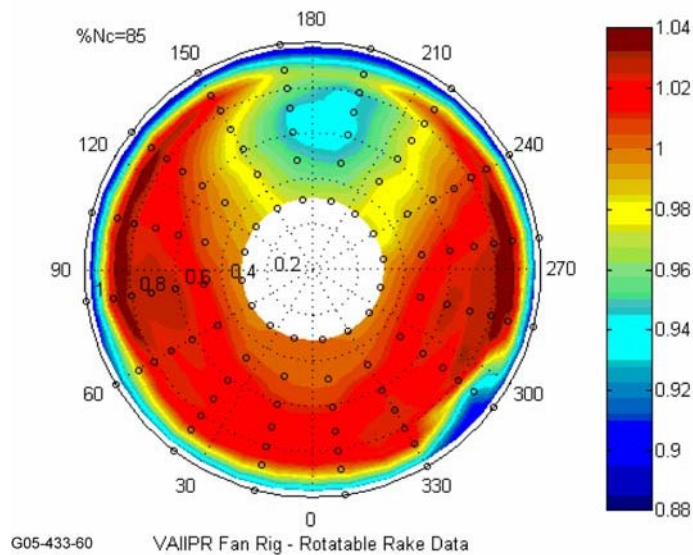
Figure 54.—Total pressure contour for 85 percent N_c (above –7 percent op-line) with AFC off.

Figure 54 through Figure 57 show the impact of AFC on the total pressure near the fan duct face for the higher speed conditions, 85 percent N_c. These figures show the 180° position as the 12 o'clock position or TDC. Comparing these figures, the stationary inlet distortion patterns for the conditions of AFC Off, AFC Fwd, AFC On, and AFC max, indicate the gradual removal or elimination of the low-pressure 1-per-rev distortion with the addition of active flow control. The CDI corresponding the AFC conditions for this 85 percent N_c test condition are, 0.03581 (Figure 54), 0.03688 (Figure 55), 0.02121 (not shown), 0.01396 (Figure 56), and 0.01393 (Figure 57). The noise data at BPF and multiples of BPF was shown to increase with this reduction in circumferential distortion.
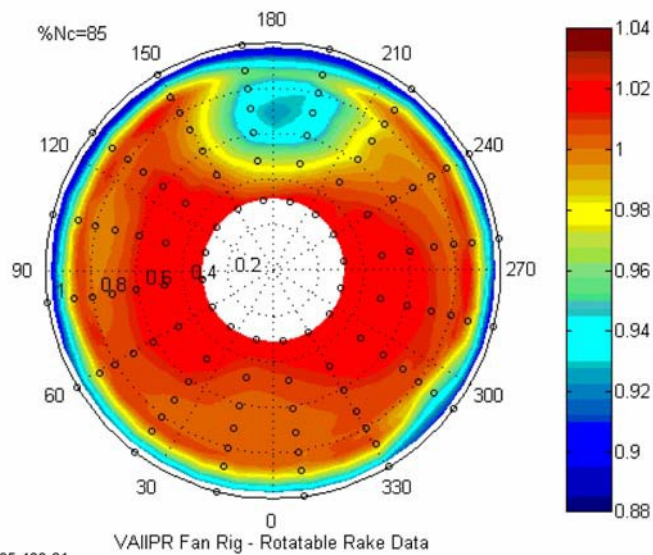
Figure 55.—Total pressure contour for 85 percent N_c (above −7 percent op-line) with AFC fwd.
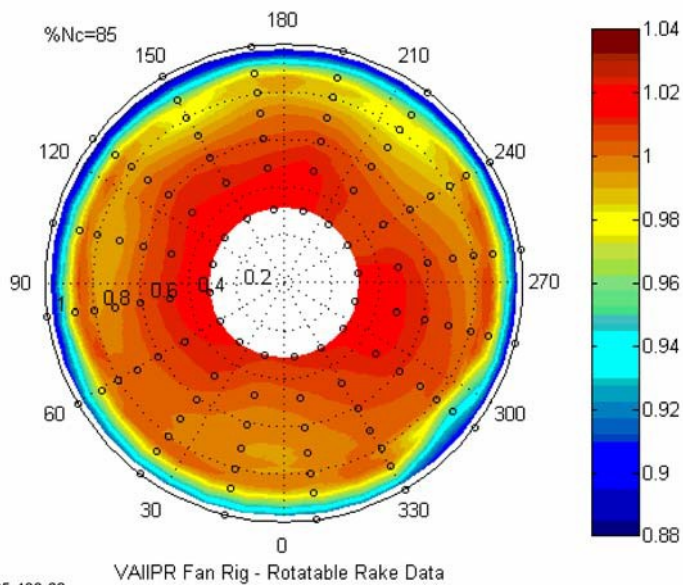
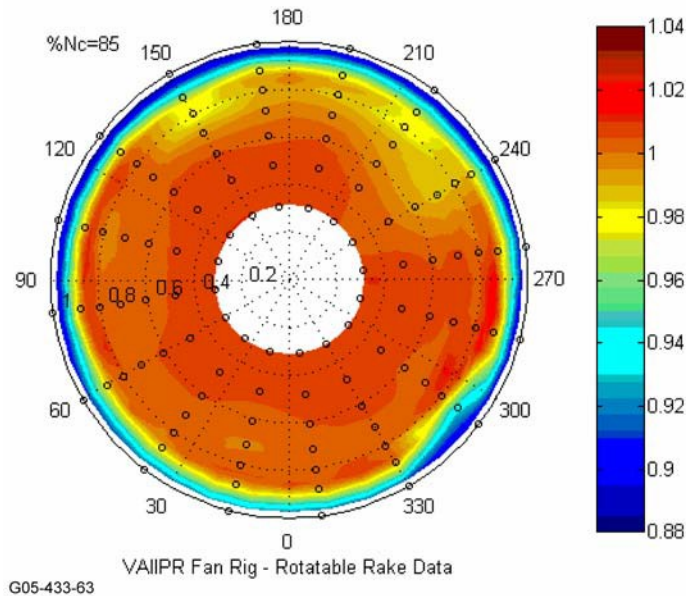Figure 56.—Total pressure contour for 85 percent N_c (above −7 percent op-line) with AFC on.

Figure 57.—Total pressure contour for 85 percent N_c (above
–7 percent op-line) with AFC max.

4.4   Introduction of IGVs

Figure 58 shows a comparison of the narrowband pressure spectrum of the circumferentially averaged pressures for three different fan schedules representing the effect of IGV turning angle at a typical approach condition, 63 percent N_c at the –7 percent op-line conditions. The fan schedule (Fan Schedules 1 and 2) represents IGV angles of 35.2°, 30.3°, and 20.2 °, respectively where opening the fan IGVs (decreasing IGV angle) results in increasing the fan inlet corrected flow and fan pressure ratio (see Figure 13). The broadband and tonal noise levels are both reduced as might be expected, based on the changes in engine operating conditions.

Spinning mode estimates corresponding to the three IGV settings in Figure 58 are shown in Figure 59. This figure shows the reduction with IGV angle in the m = 0 and the m = 3 modes in addition to a reduction in the overall broadband levels of all the indicated modes. The m = 0 and m = 3 have been attributed to fan/IGV interactions. This behavior is consistent with the narrowband noise results that also show a corresponding reduction in both BPF tones and broadband noise. Results from the Virtual Array are shown in Figure 60. The Virtual Array processing has identified the fan/IGV interaction mode, m = –16, as a dominant mode as well as the m = 3 fan/IGV interaction mode. The Virtual Array seeks dominant interactions, spinning modes, in the duct and has identified the dominant modes consistent with the evenly spaced array results in Figure 59. The noise floor in the Virtual Array results has been reduced with IGV setting.

4.5   Introduction of Upstream Struts

The effect of upstream struts is shown in Figure 61 for the 63 percent N_c engine operating condition. The engine configurations that make up this comparison were Build 4 (struts) and Build 5 (no struts), see Figure 4. These tests were conducted about 1 month apart. The effect of the three relatively thick upstream struts can be seen primarily to impact some low frequency broadband noise, 3 dB differences between 1 and 4 kHz, and high frequency noise above 10 kHz. These added noise levels in the duct may be attributed to increased turbulence from the wakes of these struts. Additional data is needed to further quantify the relative differences in the internal acoustic field due to the presence of these struts. There does not appear to be any significant changes in BPF and 2*BPF tone noise. Modal comparisons were not generated for this condition because of the absence of a 1-rev signal in the Build 4 test results.
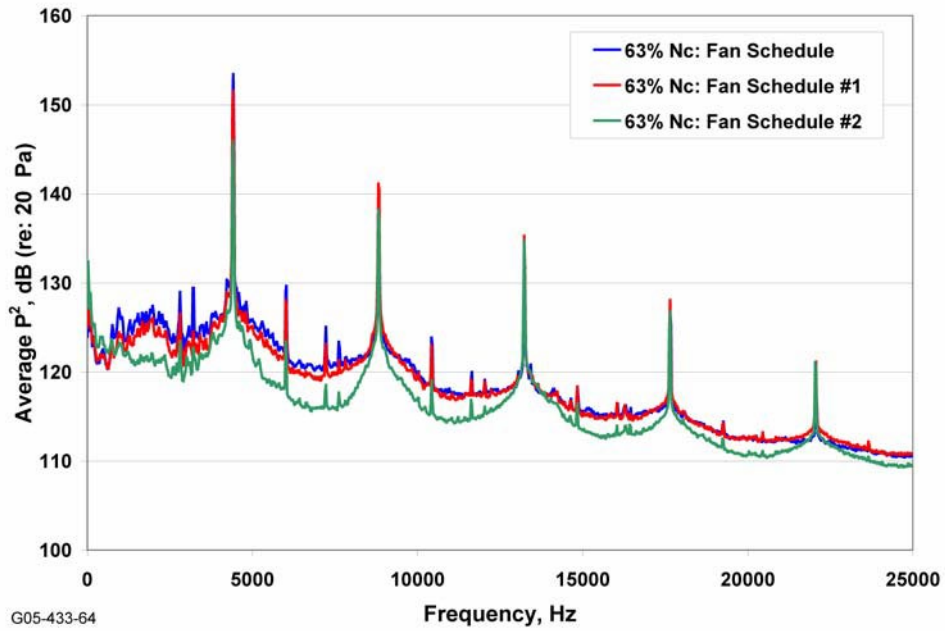
Figure 58.—The effect of IGVs on the circumferentially averaged P^2 levels from the 32-sensor array at 63 percent N_c (–7 percent op-line) with AFC on.
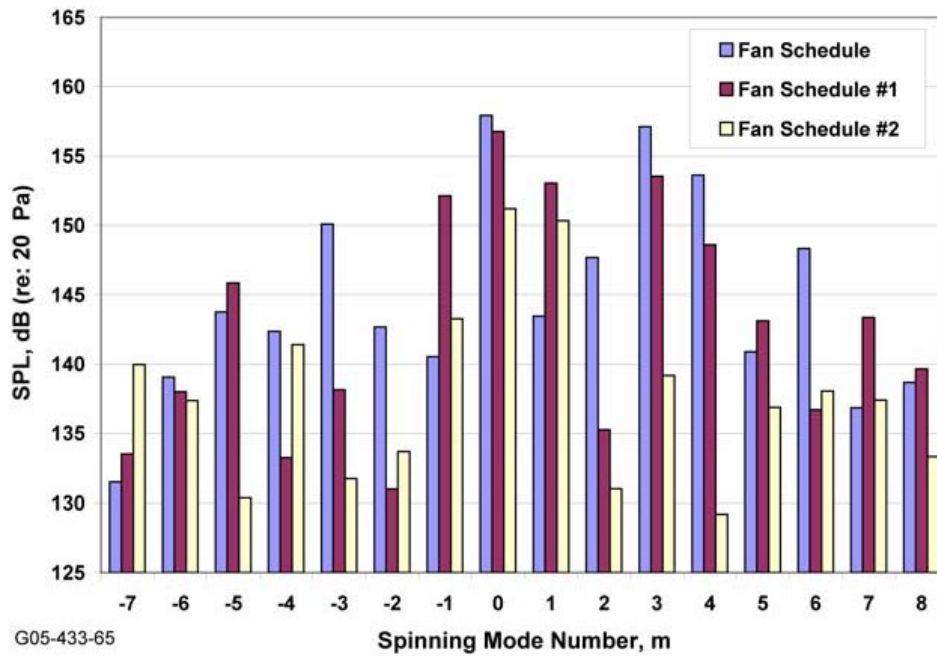
Figure 59.—Spinning mode content at 63 percent N_c (–7 percent op-line) with AFC on and all IGV settings.
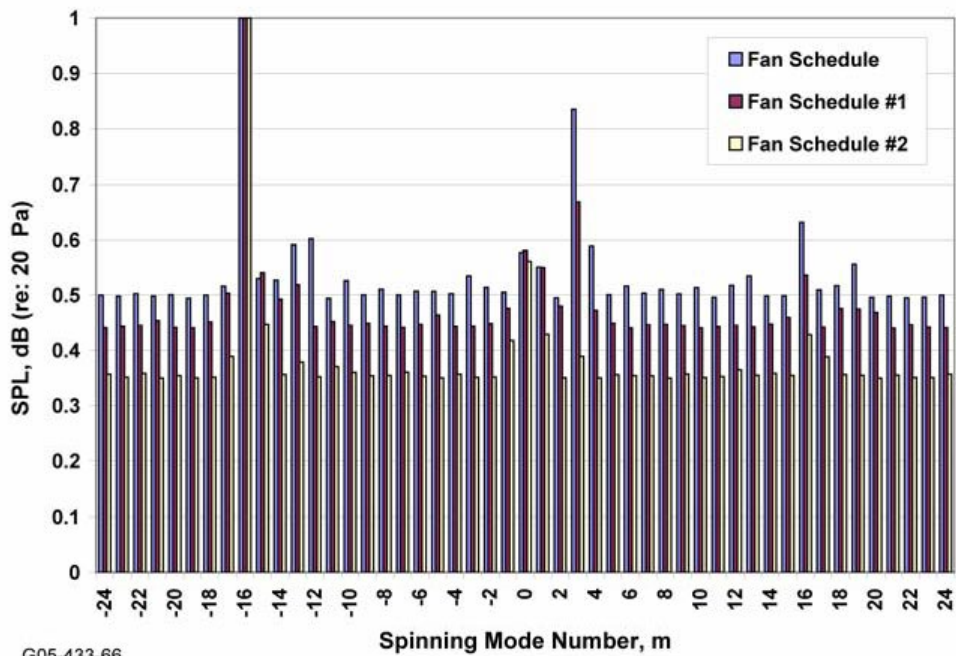
G05-433-66

Figure 60.—Spinning mode content from the virtual array at 63 percent N_c (–7 percent op-line) with AFC on and all IGV settings.

G05-433-67

Figure 61.—the effect of struts, Build 4, on the circumferentially averaged P^2 levels from the 32-sensor array at 85 percent N_c (–7 percent op-line).

4.6   Attenuation of the Inlet Design

Sensors located in the inlet of the duct potentially show how the pressure field as measured near the fan face is attenuated as it propagates upstream and out the inlet of the serpentine inlet. Figure 7 shows the two sensor locations at the inlet, one at 12 o'clock and 6 o'clock. Figure 62 shows the spectral results fo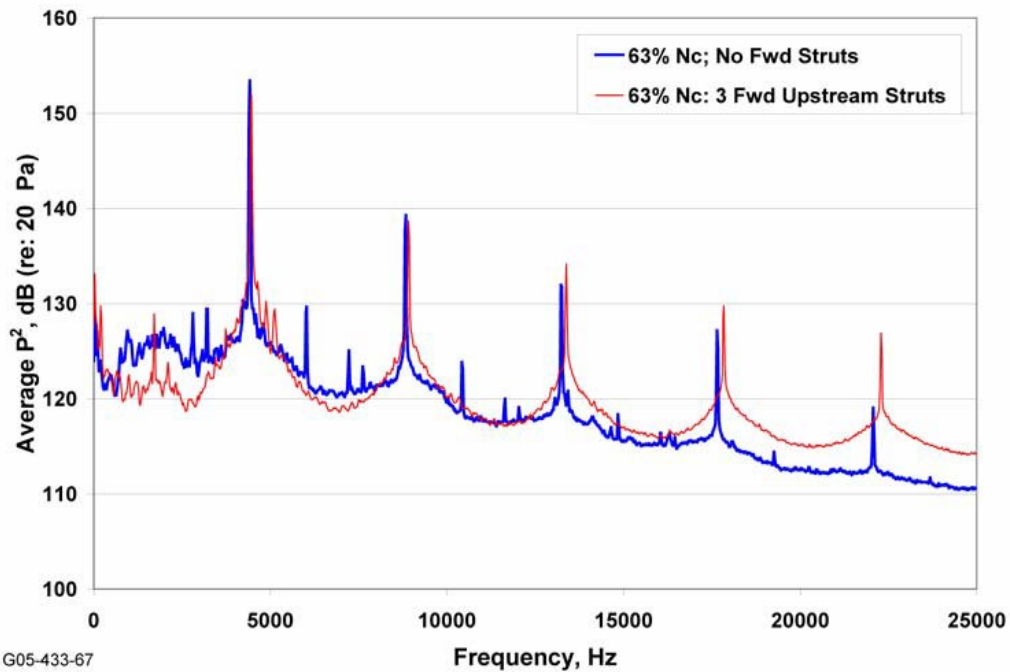r the 63 percent N_c speed setting comparing the data from 12 o'clock and 6 o'clock sensors for AFC on and AFC off. As shown, the two sensors compare reasonably well at a given active flow condition with slight differences near the BPF tone. These sensors are not expected to be identical due to their differences in proximity to the various sources in the duct and location relative to the propagating acoustic field in the duct. Not clear from this figure is the observation that the AFC on condition resulted in increased pressure levels at both sensors at blade pass consistent with most of the previously presented data in the circumferential array near the fan. Also consistent with the circumferentially averaged p^2 levels is the broadband noise reduction with AFC observed in both sensors. As a result of the similarity in spectral features between the 12 o'clock and 6 o'clock sensors, only the results from the 12 o'clock sensor will be presented to illustration the effect of the serpentine inlet on the noise.

Figure 63 through Figure 65 show the effect of the serpentine inlet on the upstream propagating sound field. Each of these figures show the circumferentially averaged p^2 levels near the fan face with AFC off and the 12 o'clock inlet sensor with AFC off for 63, 75, and 85 percent N_c (all just below the –7 percent op- line), respectively. In addition, each figure contains the results at the 12 o'clock sensor for AFC on. These figures clearly show that the inlet has a significant effect, as expected, on the upstream propagation of noise. Also as expected, the benefits of this reduction in the line of sight from the serpentine inlet are more pronounced at the higher frequencies. The high frequency or low wavelength noise is more effectively attenuated due to scrubbing losses and destructive interference of the acoustic waves with the duct. In addition, the SPL differences between the inlet sensors and the circumferentially averaged fan pressures increases as the engine speed increases. The effect of AFC on the broadband levels is diminished as the speed is increased. This may be due to the increase in turbulence generated sound at the higher speed settings.
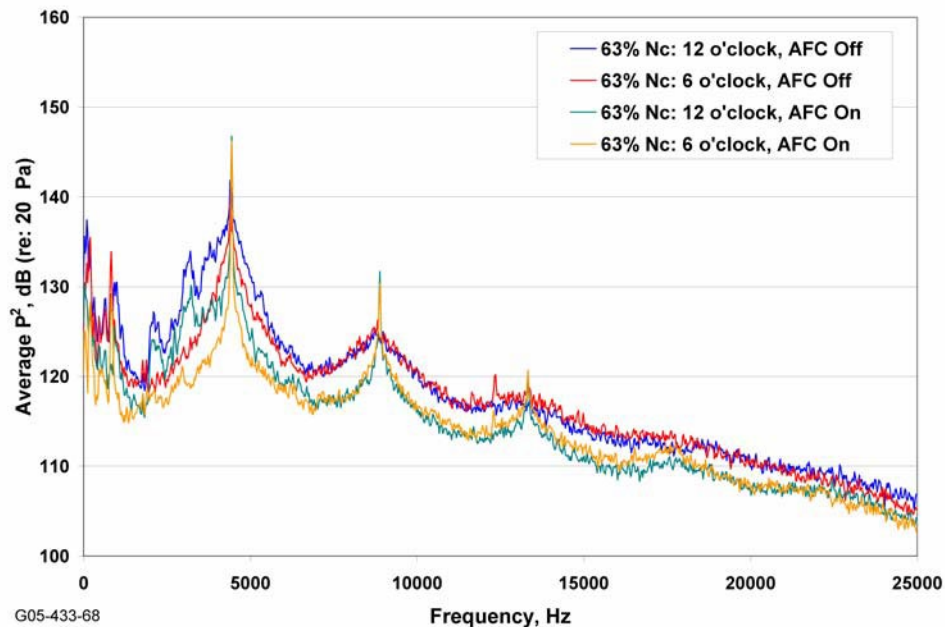
Figure 62.—The effect of serpentine inlet on the inlet noise levels comparing the 12 o'clock and 6 o'clock inlet sensors for AFC on and AFC off for 63 percent N_c (nominal op-line).
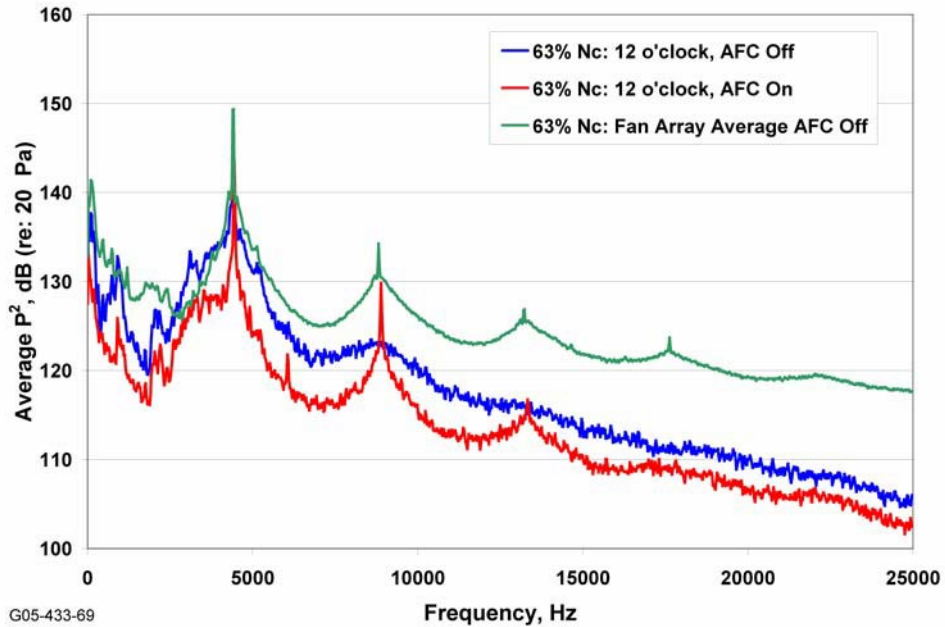
Figure 63.—The effect of serpentine inlet on the inlet noise levels as compared to the circumferentially averaged P^2 levels from the 32-sensor array near the fan at 63 percent N_c (below –7 percent op-line).
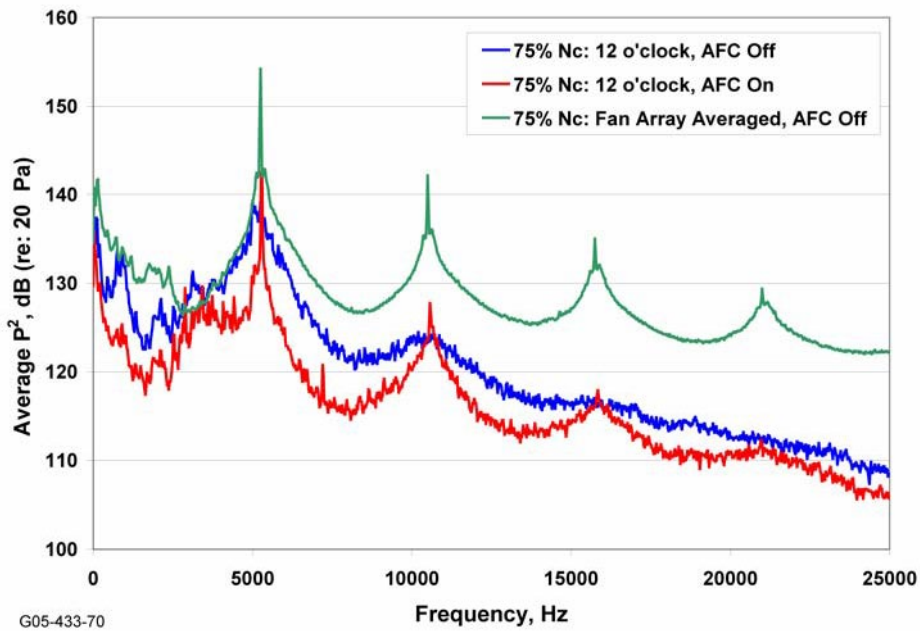
Figure 64.—The effect of serpentine inlet on the inlet noise levels as compared to the circumferentially averaged P^2 levels from the 32-sensor array near the fan at 75 percent N_c (below –7 percent op-line).
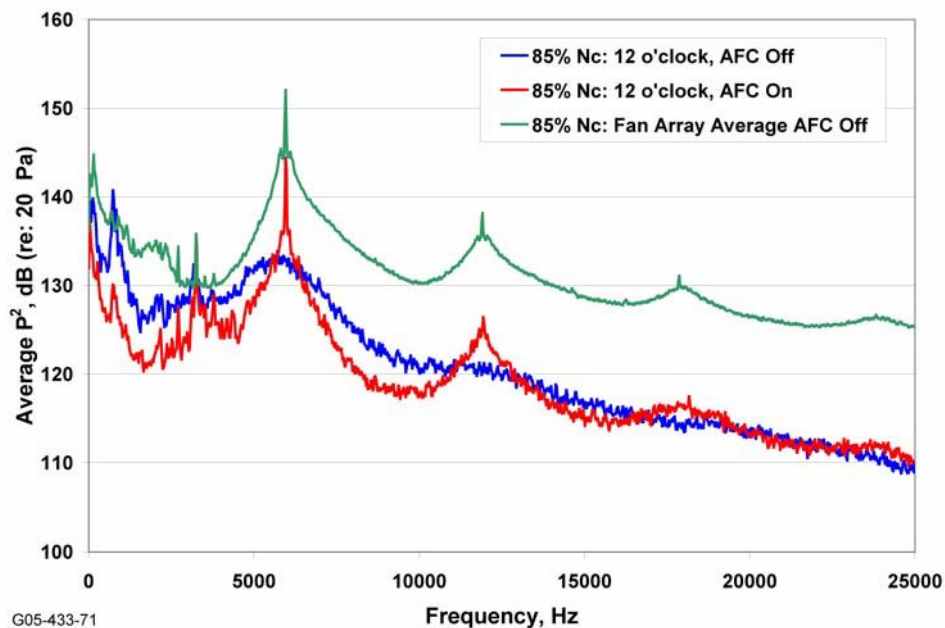
Figure 65.—The effect of serpentine inlet on the inlet noise levels as compared to the circumferentially averaged P^2 levels from the 32-sensor array near the fan at 85 percent N_c (below –7 percent op-line).

4.7   Smart Vanes

Smart Vanes were used to control the inflow from the IGVs to the fan and to eliminate actuation of the IGV. The details of the smart vane design have been omitted for proprietary reasons. Due to schedule changes, limited acoustic data was acquired for this engine build (Build 6). Figure 66 shows a comparison between different IGV flow conditions on the measured pressures at the circumferential array for 63 percent N_c on the –7 percent op-line. Epsilon represents the percentage of flow from the IGV relative to the core flow and is representative of the amount of closure on the IGV. The more the IGV is closed the more fan flow is increased and the higher the fan pressure ratio. The precise correlation between epsilon and the IGV setting was not established by Honeywell/Government team at the time of final documentation of this work; however, an epsilon of ~3 percent is expected to correlate to about 12° closure of the IGV vane. The effective vectoring angle will be determined by comparing the compressor map data to the compressor map obtained with mechanically articulated vanes during Build 5 of the VAIIPR test program. The behavior at BPF and surrounding broadband levels from the Smart Vane results in Figure 66 appear to match that shown previously in Figure 58 where the higher closure angle (higher epsilon) positively correlates with increased broadband and tonal levels. Higher multiples of the BPF tone appear to match identically between the two smart vane conditions shown and there is less difference between broadband levels.

There is no overlapping condition from the previous builds for comparison with this acoustic data from Build 6.
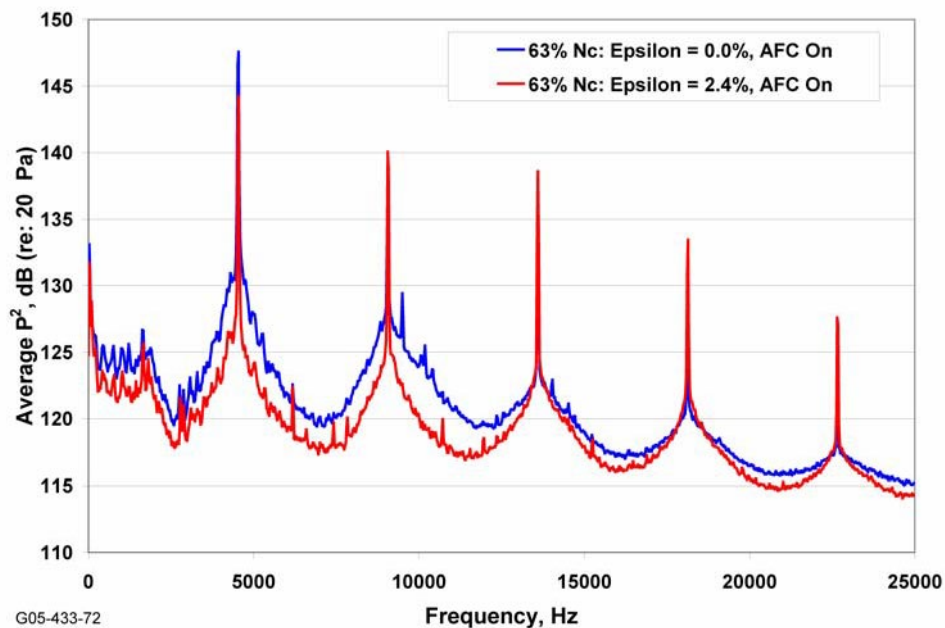
Figure 66.—The effect of smart vanes on the circumferentially averaged P^2 levels from the 32-sensor array at 63 percent N_c (–7 percent op-line).

5.0   Conclusions

Internal fan noise measurements were made near the fan and at the inlet of a serpentine inlet during performance, operability, and durability testing of the PRDA VI fan under the VAIIPR program. The VAIIPR program was sponsored by the Air Force and run by Lockheed Martin with the assistance of Honeywell. The VAIIPR program provided a unique opportunity to collect internal noise data to characterize various fan interaction mechanisms and the inflow effects on the fan in parallel with an extensive fan performance and aeroelastic characterization effort. In addition, it provided an opportunity to qualitatively assess the propagation of fan generated noise through a serpentine inlet with and without various levels of active flow control in the inlet.

The effects of inlet distortion, IGVs, upstream struts, and Smart Vane technology (flow through a coanda surface is used to replace mechanically actuated IGVs) on fan interaction noise and the attenuation of this noise resulting from the serpentine inlet were assessed with a circumferential array of dynamic pressure sensors just upstream of the fan and IGVs and sensors in the inlet of the serpentine inlet. Between NASA Langley and Honeywell, a total of 34 PCB dynamic pressure sensors were available with signal conditioning to support VAIIPR noise testing over a several month period at Wright-Patterson Air Force Base. A Dewetron data acquisition system was leased and assembled with ICP modules for the PCBs. This system was configured to allow for remote acquisitioning via Ethernet cabling to a control room near the CRF. The single Ethernet cable eliminated the need for 150-ft sensor cabling and potential phase errors introduced by such cable lengths and connectors.

Honeywell designed an array of 32 sensors spaced non-uniformly around the circumference and located just upstream of the IGVs and the fan face. The Virtual Array concept was developed by Honeywell as a means for identifying the spinning mode content in a circular duct under conditions where the number of actual sensors are less than ideal or to survive the unexpected loss of multiple sensors during testing. Simulations of a few design patterns using the Virtual Array processing indicated that 32 sensors could adequately resolve spinning mode orders just beyond the rotor alone mode for this 22 bladed fan (m = 22) at BPF. Previous evaluations of the Virtual Array concept using Honeywell engine data indicated that this approach was valid when the number of actual sensors was at a minimum equal to the

number of desired modes divided by 1.5 or 2/3 of the sensors could be lost from an ideal array. There were numerous test cases where multiple sensors were lost during VAIIPR noise recordings and therefore exceeded the previously validated range of its useful application. As a result, an evenly spaced array of 16 sensors (subset of the 32 non-uniformly spaced sensors) from the Virtual Array of 32 sensors were used for the traditional 2-D FFT approach to modal decomposition. This sensor count and method knowingly resulted in many aliased modes to decipher. It was also hoped that the uniformly spaced array would initially identify modes of significance to be used as initial input for the Virtual Array spectral estimation of spinning modes.

A flow spacer was designed and fabricated for the acoustic instrumentation. On-site support from an acoustic engineer and an acoustic technician was provided at Wright-Patterson during the initial acoustic build (Build 4) to support the installation of acoustic hardware and initial acoustic testing. A calibration of the initial acoustic instrumentation and data acquisition system setup was complete prior to Build 4. Subsequent builds (Builds 5 and 6) did not require acoustic support due to coordination between the Honeywell team and Wright-Patterson engineers and the simple remote data acquisitioning established by Honeywell during the Build 4 set-up.

Acoustic data collection spanned about a 2 month time period. Time histories were transferred to a USB transfer drive and brought to Honeywell for processing. Data from the fan array were processed and presented in the form of spatially averaged squared pressures versus frequency content as well as spinning mode amplitude versus mode number. The inlet sensor narrowband results were also presented in a similar manner

Using circumferentially averaged p^2 levels, the measured noise data indicate that AFC in the serpentine inlet provides significant reduction in broadband noise with the reduction occurring gradually with increasing levels of AFC. Active flow control had the effect of eliminating the natural 1/rev distortion from the serpentine inlet and reducing the amount of circumferential distortion at the fan face. Surprisingly, the introduction of AFC slightly increased the levels at the blade pass tone (BPF) and 2xBPF tone. Both findings were consistent for the typical approach, cutback, and max power settings under study. The serpentine inlet provides a significant amount of noise attenuation at high frequencies with less benefit at the BPF. The IGVs were also shown to have the effect of lowering both broadband noise and tone noise as the IGVs closed. This result may be expected because of the drop in fan flow and fan pressure ratio that corresponds to the IGV closing.

Modal results from the evenly spaced sensor array showed a strong presence of a fan IGV interaction. This interaction mode appeared as a dominant aliased mode in the modal decomposition due to the limited spinning mode resolution of the 16 sensor array (–8 to 8). For the test cases where the Virtual Array processing could be utilized, the 32-sensor array clearly identified the presence this $m = -16$ interaction mode from the fan/IGVs. In addition, an $m = 3$ fan/IGV interact was also identified under certain operating conditions. These interaction modes were shown to be reduced significantly in amplitude as the IGVs were closed. At the highest speed setting both arrays showed the presence of an $m = 22$ mode (aliased to an $m = 6$ mode in the 16 sensor array). This mode is potentially due to the rotor locked where the blade tips may be sonic or near sonic speeds. The modal amplitudes at BPF for the 63 and 85 percent speeds increased with the introduction of AFC consistent with the averaged p^2 results confirming the trends in the spectral data at the blade pass tones. The 75 percent N_c condition resulted in a more expected reduction in modal amplitude with AFC. An explanation for these trends is currently unavailable.

The modal processing from both the uniformly spaced array of 16 sensors and the non-uniformly spaced array of 32-sensors where viable appears to have reasonably identified interaction modes consistent with potential noise sources in the duct. The strong presence of fan/IGV interaction modes suggests potentially why this arrangement is not utilized in commercial power plants. Absolute modal amplitudes may be suspect due to the poor performance of some and the loss of several sensors throughout the duration of VAIIPR noise testing. To further assess the modal behavior from the VAIIPR noise measurements it may be insightful to reformulate the problem as a beam-forming problem and apply traditional beam-forming techniques to the measured data. This approach would be more amenable to deconvolution methods that may significantly improve array performance.

Appendix A.—Abbreviations and Acronyms

AFB	Air Force Base
AFC	Active Flow Control
AIP	Aerodynamic Interface Plane
AOA	angle of attack
B	Number of Rotating or Fan Blades
BNC	Coaxial Connector Type
CDI	Circumferential Distortion Index
CFD	Computational Fluid Dynamics
CRF	Compressor Research Facility
EVNRC	Engine Validation and Noise Reduction Concepts
FFT	Fast Fourier Transform
IGVs	Inlet Guide Vanes
m	Spinning Mode Order
Mn	Mach number
N_c	corrected speed
NASA	National Aeronautics and Space Administration
NSMS	Non-Intrusive Stress Management System
OGV	Outlet Guide Vane
p^2	Squared Pressure
PCB	PCB Piezotronics, Inc.
PRDA VI	Program Research and Development Announcement VI
RASER	Revolutionary Aero Space Engine Research
RPM	revolutions per minute
SPL	sound pressure level
TDC	top-dead center
UAV	Uninhabited Air Vehicle
V	Number of Vanes or Harmonic Content from Tyler-Sofrin Equation
VAIIPR	Versatile Active Integrated Inlet/Fan for Performance and Durability
ε	IGV flow injection relative to core flow, percent
γ	ordinary coherence function

References

1. Smith, W., "Pressure Losses in Ducted Flows," The Butterworth Group, London, U.K., 1971.
2. Anderson, Jason M., "Non-Intrusive Sensing and Feedback Control of Serpentine Inlet Flow Distortion," Dissertation submitted to the Faculty of the Virginia Polytechnic Institute and State University in partial fulfillment of the requirements for the degree of Doctor of Philosophy in Mechanical Engineering, April 2003.
3. Anderson, B.H., and Gibb, J., "Study on Vortex Generator Flow Control for the Management of Inlet Distortion," Journal of Propulsion and Power, Vol. 9, No. 3, pp. 420–430, 1993.
4. Tyler J.M., and Sofrin T.G.," Axial flow compressor noise studies, theoretical and computational fluids dynamics," SAE, 1961.
5. Groeneweg, J.F., Sofrin, T.G., Rice, E.J. and Gliebe, P.R., "Turbomachinery Noise," In: Hubbard, H.H., eds., Aeroacoustics of Flight Vehicles: Theory and Practice, Volume 1: Noise Sources, NASA Reference Publication 1258, Vol. 1, 1991.
6. Envia, E., Wilson, A.G., and Huff, D.L. and Gliebe, P.R. "Fan Noise: A Challenge to CAA," International Journal of Computational Fluid Dynamics, Vol. 18, pp. 471–480, August 2004.
7. Pickett, G.F., Sofrin, T.G., and Wells, R.W., "Method of Fan Sound Mode Structure Determination – Final Report," NASA CR–1352993, 1977.
8. Moore, C.J., "Measurement of Radial and Circumferential Modes in Annular and Circular Fan Ducts," J. Sound & Vibration, Vol. 62, No. 2, pp. 235–256, Jan. 22, 1979.
9. Cicon, D.E., Sofrin, T.G., and Mathews, D.C., "Investigation of Continuously Traversing Microphone System for Mode Measurements," NASA CR-168040, 1982.
10. Joppa, P.D., "Acoustic Mode Measurements in the Inlet of a Turbofan Engine," J. Aircraft, Vol. 24, No. 9, pp. 587–593, Sep., 1987.
11. S.S. Reddie, "Multiple source location: a digital approach," IEEE Trans. On AES, vol. 15, No. 1, pp. 95–105, Jan 1979.
12. L. Withers, Jr. "Piece wise Root-Music," ICASSP 91, 1991.
13. Michalke, A., Arnold, F., and Holste, F., "On the Coherence of the Sound Field in a Circular Duct with Uniform mean Flow," Journal of Sound and Vibration, Vol. 190 (2), pp. 261–271, 1996.

1. REPORT DATE *(DD-MM-YYYY)* 01-12-2012	2. REPORT TYPE Final Contractor Report	3. DATES COVERED *(From - To)* September 2004 to September 2005

4. TITLE AND SUBTITLE
Noise Measurements of the VAIIPR Fan

5a. CONTRACT NUMBER
NAS3-01136

5b. GRANT NUMBER

5c. PROGRAM ELEMENT NUMBER

6. AUTHOR(S)
Mendoza, Jeff; Weir, Don

5d. PROJECT NUMBER

5e. TASK NUMBER
Task 6

5f. WORK UNIT NUMBER
WBS 561581.02.08.03.18.11

7. PERFORMING ORGANIZATION NAME(S) AND ADDRESS(ES)
Honeywell Aerospace
111 S. 34th Street
P.O. Box 52180
Phoenix, AZ 85072180

8. PERFORMING ORGANIZATION REPORT NUMBER
E-18545

9. SPONSORING/MONITORING AGENCY NAME(S) AND ADDRESS(ES)
National Aeronautics and Space Administration
Washington, DC 20546-0001

10. SPONSORING/MONITOR'S ACRONYM(S)
NASA

11. SPONSORING/MONITORING REPORT NUMBER
NASA/CR-2012-217809

12. DISTRIBUTION/AVAILABILITY STATEMENT
Unclassified-Unlimited
Subject Categories: 71 and 02
Available electronically at http://www.sti.nasa.gov
This publication is available from the NASA Center for AeroSpace Information, 443-757-5802

13. SUPPLEMENTARY NOTES

14. ABSTRACT
This final report has been prepared by Honeywell Aerospace, Phoenix, Arizona, a unit of Honeywell International, Inc., documenting work performed during the period September 2004 through November 2005 for the National Aeronautics and Space Administration (NASA) Glenn Research Center, Cleveland, Ohio, under the Revolutionary Aero-Space Engine Research (RASER) Program, Contract No. NAS3-01136, Task Order 6, Noise Measurements of the VAIIPR Fan. The NASA Task Manager was Dr. Joe Grady, NASA Glenn Research Center, Mail Code 60-6, Cleveland, Ohio 44135. The NASA Contract Officer was Mr. Albert Spence, NASA Glenn Research Center, Mail Code 60-6, Cleveland, Ohio 44135. This report focuses on the evaluation of internal fan noise as generated from various inflow disturbances based on measurements made from a circumferential array of sensors located near the fan and sensors upstream of a serpentine inlet.

15. SUBJECT TERMS
Fans; Noise

16. SECURITY CLASSIFICATION OF:			17. LIMITATION OF ABSTRACT	18. NUMBER OF PAGES	19a. NAME OF RESPONSIBLE PERSON STI Help Desk (email:help@sti.nasa.gov)
a. REPORT U	b. ABSTRACT U	c. THIS PAGE U	UU	62	19b. TELEPHONE NUMBER *(include area code)* 443-757-5802